A Comprehensive Kinetic Model for the Free-Radical Polymerization of Vinyl Chloride in the Presence of Monofunctional and Bifunctional Initiators

Apostolos Krallis,[†,‡] Costas Kotoulas,[†,‡] Stratos Papadopoulos,[‡] Costas Kiparissides,[*,†,‡] Jacques Bousquet,[§] and Christian Bonardi[§]

Department of Chemical Engineering, Aristotle University of Thessaloniki, Chemical Process Engineering Research Institute, P.O. Box 472, Thessaloniki, Greece 541 24, and TotalFinaElf, Direction Scientifique, CRES-DRTE, BP22, 69360 Solaize, France

A comprehensive kinetic model is developed for the suspension free-radical polymerization of vinyl chloride (VC) initiated by a mixture of monofunctional and bifunctional initiators. The model predicts the monomer concentrations in the gas, aqueous, and polymer phases; the overall monomer conversion; the polymerization rate; the polymer chain structural characteristics (e.g., number- and weight-average molecular weights, short chain branching, and number of terminal double bonds); the reactor temperature and pressure; and the coolant flow rate and temperature in the reactor's jacket over the whole batch polymerization cycle. The capabilities of the model are demonstrated by a direct comparison of model predictions with experimental data on monomer conversion, number- and weight-average molecular weights, and reactor pressure. It is shown that high molecular weights and high polymerization rates can be obtained in the presence of a mixture of monofunctional and bifunctional initiators. Moreover, the use of bifunctional initiators results in a significant reduction of the polymerization time without impairing the final molecular weight properties of the polymer. To our knowledge, this is the first comprehensive kinetic modeling study on the combined use of monofunctional and bifunctional initiators on the free-radical suspension polymerization of VC. Taking into consideration the excellent agreement of the model predictions with the experimental measurements, the proposed model should find wide application in the design, optimization, and control of industrial poly(vinyl chloride) batch reactors.

Introduction

Poly(vinyl chloride) (PVC) is, by volume, the second largest thermoplastic manufactured in the world.[1] The world PVC demand in 1997 was about 23 million tons, and in 2002, the forecast for the next year was estimated at 28 million tons.[2] The predicted annual growth rate of world PVC demand is close to 4%. The sustainable expansion of the PVC industry is due to the high versatility of PVC as a plastic raw material together with its low price. A review of the qualitative and quantitative aspects of PVC polymerization can be found in works by Smallwood,[1] Burgess,[3] Langsam,[4] Tornell,[5] Xie et al.,[6,7] and Yuan et al.[8]

Four polymerization processes (i.e., suspension, bulk, emulsion, and solution) are commercially employed in PVC manufacturing. Approximately 80% of the total PVC production is obtained by the suspension polymerization process. In this process, droplets of liquid vinyl chloride monomer (VCM), containing oil-soluble initiator(s), are dispersed in the continuous aqueous phase by a combination of strong stirring and the use of suspending agents (stabilizers). The reaction takes place in the monomer droplets. The polymerization is carried out in large batch reactors (e.g., 150 m^3). The reactor's contents are heated to the required temperature where the initiator(s) start(s) to decompose. The polymerization reaction is strongly exothermic (i.e., 100 $kJ \cdot mol^{-1}$). Thus, the efficient removal of the reaction heat is critical for the operation of large-scale reactors.[9] The polymerization heat is transferred from the monomer droplets to the aqueous phase and then to the reactor wall, which is cooled by chilled water flowing through the reactor's jacket. In large-scale reactors, overhead condensers are employed to remove part of the reaction heat through the evaporation and subsequent condensation of the monomer. When all of the free liquid monomer has been consumed, the pressure in the reactor starts to fall as a result of the monomer mass transfer from the vapor phase to the polymer phase due to subsaturation conditions. In industrial PVC production, the reaction is usually stopped when a certain pressure drop has been recorded. Because the polymer is effectively insoluble in its own monomer, once the polymer chains are first generated, they precipitate immediately to form a separate phase in the polymerizing droplet. Thus, from a kinetic point of view, the polymerization of VCM is considered to take place in three stages.[10]

During the first stage, primary radicals formed by the thermal fragmentation of the initiator molecules rapidly react with monomer to produce the first polymer chains. During this early polymerization period, the concentration of the polymer is below its solubility limit in the monomer (i.e., the VCM conversion is less than 0.1%);

* To whom correspondence should be addressed. Tel.: +302310 99 6211. Fax: +2310 99 6198. E-mail: cypress@alexandros.cperi.certh.gr.
† Aristotle University of Thessaloniki.
‡ Chemical Process Engineering Research Institute.
§ TotalFinaElf.

10.1021/ie0498908 CCC: $27.50
Published on Web 08/31/2004

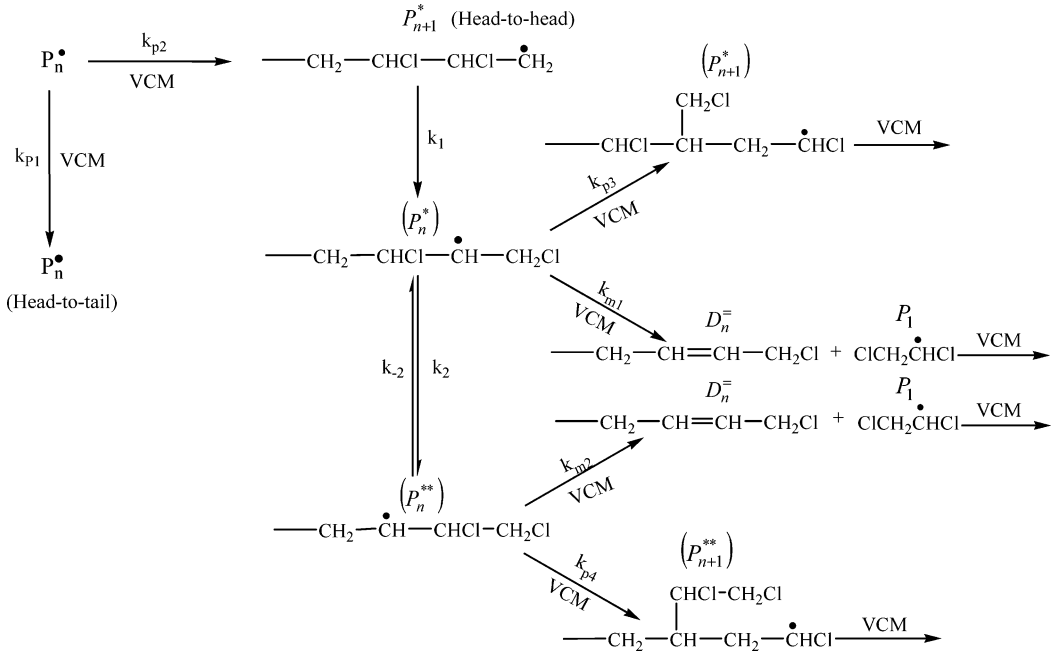

Figure 1. Formation of chloromethyl and ethyl branches and terminal double bonds (Starnes[31]).

therefore, the polymerization occurs in a single homogeneous phase.

The second polymerization stage extends from the time of the appearance of a separate polymer phase, in addition to the monomer phase, to the time at which the separate monomer phase disappears, which occurs at the fractional monomer conversion X_f. During this stage, the reaction mixture consists of four phases, namely, the monomer-rich phase, the polymer-rich phase, and the aqueous and gaseous phases. The reaction takes place in the monomer and polymer phases at different rates and is accompanied by the transfer of monomer from the monomer-rich phase to the polymer-rich phase so that the latter is kept saturated with monomer. The disappearance of the monomer-rich phase is associated with a characteristic drop in the reactor pressure.

In the third stage, at higher monomer conversions ($X_f < X < 1.0$), the polymerization proceeds exclusively in the polymer-rich phase that is swollen with the residual monomer. Thus, the monomer mass fraction in the polymer-rich phase continuously decreases as the total monomer conversion approaches its final limiting value.

In the past 30 years, several mathematical kinetic models have been developed to describe the two-phase suspension polymerization of VCM.[7,10−23] All of these studies have been limited to the development of kinetic models for single monofunctional initiators and/or mixtures of them. However, there is growing interest in the polymer industry in the use of multifunctional initiators. Multifunctional initiators usually contain two labile groups having different thermal decomposition characteristics. These initiators follow a decomposition mechanism that is completely different from the well-known mechanism of monofunctional initiators. As a result, substantially higher polymerization rates can be achieved with concomitant reductions of the batch time. In general, the kinetic mechanism of the free-radical polymerization of VCM initiated by a mixture of monofunctional and bifunctional initiators is much more complex than that for the same process initiated by a mixture of monofunctional initiators because the presence of two peroxide groups per initiator molecule leads to the formation of "live" and "dead" polymer chains ending in an unreacted peroxide group.

A limited number of reports on the kinetic modeling of vinyl monomers in the presence of bifunctional initiators have been published in the open literature.[24−29] However, all of these previous kinetic studies on bifunctional initiators focused on the free-radical homogeneous polymerization of vinyl and styrenic monomers. Therefore, this is the first attempt to model the heterogeneous free-radical polymerization of vinyl chloride initiated by a mixture of monofunctional and bifunctional (both symmetrical and unsymmetrical) initiators.

In what follows, a comprehensive kinetic mechanism is proposed for the free-radical polymerization of vinyl chloride. On the basis of the postulated kinetic mechanism, general rate functions for the production of live, inactive, and dead polymer chains in the two reaction phases (i.e., monomer-rich and polymer-rich) are derived. To follow the development of the molecular weight in the two-phase heterogeneous polymerization system, the method of moments is employed. Moreover, two additional dynamic balances are derived to account for the structural characteristics (i.e., number of short chain branches and number of double bonds) of the polymer. To account for diffusion-controlled reactions (i.e., gel, glass, and cage effects) in the VCM heterogeneous polymerization process, a comprehensive model based on the free-volume theory is employed.[7] The concentrations of VCM in the four phases (i.e., monomer-rich, polymer-rich, aqueous, and gas) are calculated by assuming that the four phases are in thermodynamic equilibrium.[23] Most values of the kinetic and thermodynamic parameters were taken from the work of Kiparissides et al.[23] A limited number of parameters (e.g., initiator decomposition rate constants) were estimated by fitting the model predictions to a comprehensive set of experimental data on monomer conversion, polymerization rate, and reactor pressure provided by ATOFINA. The excellent predictive capabilities of the proposed model makes it a unique simulation tool,

useful in the design, optimization, and control of industrial PVC batch reactors.

Mechanism of VCM Polymerization

In general, the free-radical polymerization of vinyl monomers includes chain initiation, propagation, chain transfer to monomer, and bimolecular termination reactions. However, there is strong evidence that, in the free-radical polymerization of VCM, some reactions (e.g., chain transfer to monomer, formation of short and long chain branches, etc.) involve complex kinetic mechanisms.[7] In fact, the presence of chloromethyl and ethyl short chain branches in PVC validates the conclusion that propagation reactions involve several types of radicals.[30] Figures 1−3 show in detail the mechanisms leading to the formation of chloromethyl and ethyl branches and terminal double bonds, the formation of long chain branches and internal bouble bonds, and the formation of short chain branches via a backbiting reaction mechanism, respectively. According to Xie et al.,[7] Starnes et al.,[30] and Starnes,[31] a comprehensive kinetic mechanism for the free-radical polymerization of VCM involves the following elementary reactions:

Decomposition of Initiator

$$I_m \xrightarrow{k_d} 2R \tag{1}$$

Formation of Primary Radicals

$$R + M \xrightarrow{k_I} P_1 \tag{2}$$

Head-to-Tail Propagation

$$P_n + M \xrightarrow{k_{p1}} P_{n+1} \tag{3}$$

Head-to-Head Propagation

$$P_n + M \xrightarrow{k_{p2}} P^*_{n+1} \tag{4}$$

Formation of Chain Defect Structures

Chlorine shift reactions

$$P^*_n \xrightarrow{k_1} (P^*_n) \tag{5}$$

$$(P^*_n) \underset{k_{-2}}{\overset{k_2}{\leftrightarrow}} (P^{**}_n) \tag{6}$$

Formation of chloromethyl branches

$$(P^*_n) + M \xrightarrow{k_{p3}} (P^*_{n+1}) \tag{7}$$

Formation of ethyl branches

$$(P^{**}_n) + M \xrightarrow{k_{p4}} (P^{**}_{n+1}) \tag{8}$$

1,5-Shift backbiting reaction

$$P_n \xrightarrow{k_b} P'_n \tag{9}$$

Head-to-tail addition

$$P'_n + M \xrightarrow{k_{pa1}} (P'_{n+1}) \tag{10}$$

Formation of dichlorobutyl branches

$$(P'_n) + M \xrightarrow{k_{pa2}} BB \tag{11}$$

Six-center backbiting reaction

$$(P'_n) \xrightarrow{k'_b} (P''_n) \tag{12}$$

Formation of 1,3-diethyl branch pair

$$(P''_n) + M \xrightarrow{k_{pa3}} DEB \tag{13}$$

Chain Transfer to Monomer Reactions

$$(P^*_n) + M \xrightarrow{k_{m1}} D^{=}_n + P_1 \tag{14}$$

Formation of terminal double bonds

$$(P^{**}_n) + M \xrightarrow{k_{m2}} D^{=}_n + P_1 \tag{15}$$

Formation of internal double bonds

$$P_m + M \xrightarrow{k_{m3}} \overline{\overline{D}}_m + P_1 \tag{16}$$

Formation of Long Chain Branches

Hydrogen abstraction

$$P_n + D_m \xrightarrow{k_h} D_n + P'_m \tag{17}$$

1,6-Shift backbiting reaction

$$P_m \xrightarrow{k''_b} P'_m \tag{18}$$

Formation of long chain branches

$$P'_m + M \xrightarrow{k_{p5}} P'_{m+1} \tag{19}$$

Termination by Combination

$$P_n + P_m \xrightarrow{k_{tc}} D_{n+m} \tag{20}$$

Termination by Disproportionation

$$P_n + P_m \xrightarrow{k_{td}} D_n + D_m \tag{21}$$

Inhibition

$$P_n + Z \xrightarrow{k_z} D_n + Z^{\bullet} \tag{22}$$

$$Z^{\bullet} + Z^{\bullet} \xrightarrow{k_{zt}} Z \tag{23}$$

The symbols I_m, Z, and M denote the monofunctional initiator, inhibitor, and monomer molecules, respectively. The symbols P_n and D_n are used to identify live and dead polymer chains, respectively, containing n monomer units. The symbols P^*_n, (P^*_n) and (P^{**}_n) denote the live polymer chains formed via a head-to-head emplacement of monomer. The symbol P'_m identifies the intermediate macroradical species produced via the hydrogen abstraction reaction. The symbols $D^{=}_n$ and $\overline{\overline{D}}_n$ denote dead polymer chains with terminal and internal double bonds, respectively. Finally, the symbols P'_n, (P'_n), and (P''_n) denote the intermediate live polymer chains that lead to the formation of DEB (1,3-diethyl branch pair) and BB (dichlorobutyl branch) short chain branches. All of the above reactions can occur in both monomer and polymer phases.

The kinetic mechanism illustrated above shows that different types of live polymer chains [e.g., P_n, P^*_n, (P^*_n), (P^{**}_n), P'_m, etc.] are produced during vinyl chloride polymerization. However, most of the relevant kinetic rate constants (i.e., k_{p2}, k_{p3}, k_{p4}, k_{p5}, k_{pa1}, k_{pa2}, k_{pa3}) are

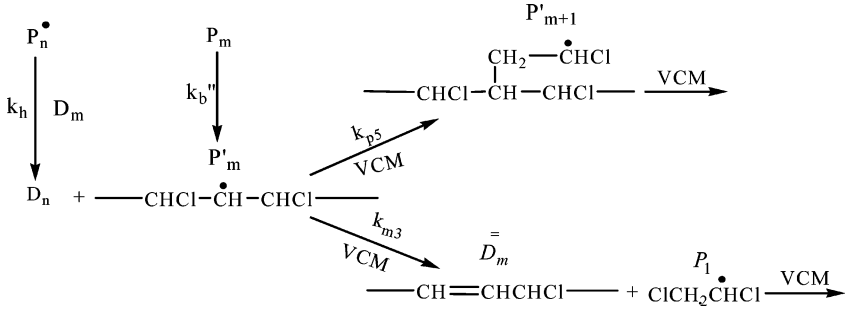

Figure 2. Formation of long chain branches and internal double bonds (Starnes et al.[30]).

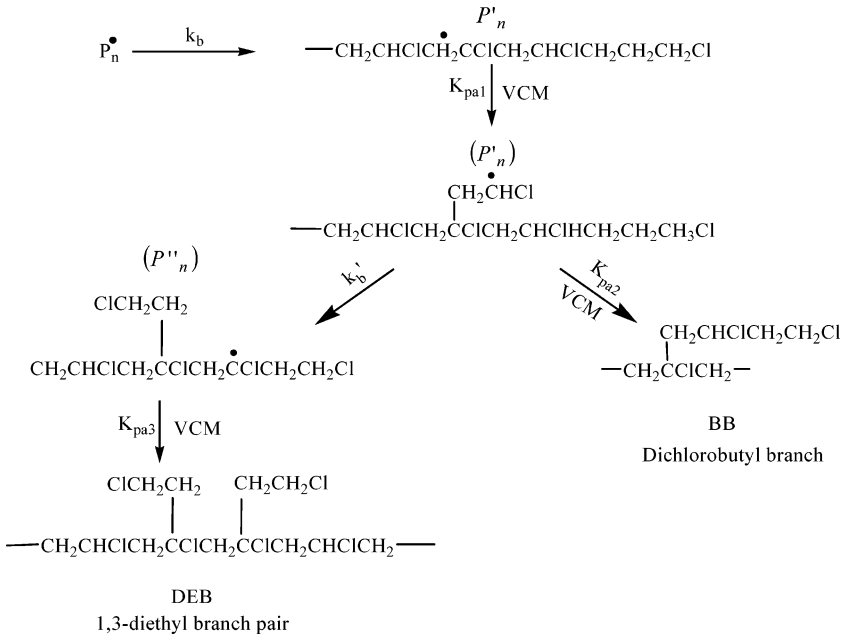

Figure 3. Formation of short chain branches (Starnes et al.[30]).

not known, and the concentration of all intermediate species cannot be measured. Taking into account the facts that most of the live polymer chains undergo tail addition to monomer[30] and that limited information is available on the numerical values of the kinetic rate constants, all of the propagation reactions (eqs 3, 4, 7, 8, 10, 11, 13, and 19) were lumped into a single propagation reaction. For the same reason, the three chain transfer to monomer reactions (eqs 14−16) were lumped into one chain transfer to monomer reaction.[23]

According to the work of Starnes et al.,[30] different types of short chain branches can be produced via backbiting reactions. The DEB structure is always produced in low concentrations, so it can be ignored.[30] Furthermore, the 1,6-shift backbiting reaction is ordinarily slower than the analogous 1,5-shift backbiting reaction. Thus, a single backbiting reaction was employed to account for the formation of BB branches.

Taking into account all of the above remarks, the above detailed kinetic mechanism (eqs 1−23) can be recast into a more realistic and simpler kinetic scheme that can be employed to predict the VCM consumption rate and the main molecular features of the PVC chains (e.g., number- and weight-average molecular weights, short and long chain branches, double bonds, etc.).[7,23]

Using the above simplifications, a comprehensive kinetic model was developed for the free-radical polymerization of VCM initiated by a mixture of monofunctional and bifunctional initiators.

Comprehensive Kinetic Mechanism and Polymerization Rate Functions

A typical molecular structure of an unsymmetrical bifunctional initiator is depicted below

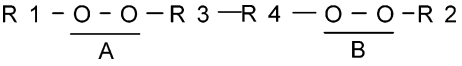

where the symbols R1, R2, R3, and R4 represent different hydrocarbon ligands and the oxygen−oxygen atoms represent the peroxide groups. In general, the two O−O groups (marked by the letters A and B) will have different decomposition activation energies. Thus, the decomposition reaction scheme for an unsymmetrical bifunctional initiator molecule can be represented as follows

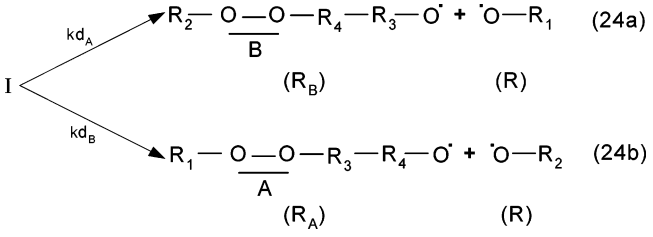

where k_{dA} and k_{dB} denote the decomposition rates of the two labile groups A and B, respectively. It is apparent

Table 1. Live, Inactive, and Dead Polymer Chains

species	description
P_n	$\bullet - - - - - - - -]$	live polymer chain
Q_n	$\bullet - - - - - - - R_A$	live polymer chain with one terminal peroxide group (A)
S_n	$\bullet - - - - - - - R_B$	live polymer chain with one terminal peroxide group (B)
T_n	$\bullet - - - - - - - - \bullet$	diradical live polymer chain
U_n	$[- - - - - - - - - - - - R_A$	inactive polymer chain with one terminal peroxide group (A)
V_n	$[- - - - - - - - - - - - R_B$	inactive polymer chain with one terminal peroxide group (B)
W_n	$R_A - - - - - - - - - - R_B$	inactive polymer chain with two terminal peroxide groups (A and B)
U'_n	$R_A - - - - - - - - - - R_A$	inactive polymer chain with two terminal peroxide groups (A and A)
V'_n	$R_B - - - - - - - - - - R_B$	inactive polymer chain with two terminal peroxide groups (B and B)
D_n	$[- - - - - - - - - - - -]$	dead polymer chain

from the decomposition reaction scheme in eqs 24a and 24b that three kinds of primary radicals (i.e, R_A, R_B, and R) are produced. The primary radicals R_A and R_B each contain one undecomposed peroxide group of type A and B, respectively. The R_A and R_B primary radicals can undergo further decomposition according to the reaction scheme in eqs 25a and 25b

$$\underset{}{R_A} \xrightarrow{k_{dA}} \underset{(R')}{{}^{\bullet}O - R_3 - R_4 - O^{\bullet}} + \underset{(R)}{{}^{\bullet}O - R_1} \qquad (25a)$$

$$\underset{}{R_B} \xrightarrow{k_{dB}} \underset{(R')}{{}^{\bullet}O - R_3 - R_4 - O^{\bullet}} + \underset{(R)}{{}^{\bullet}O - R2} \qquad (25b)$$

where R′ denotes the diradical species produced via the decomposition of the R_A and R_B radicals.

In the present study, the symmetrical bifunctional initiator DIPND [1,3-di(2-neodecanoylperoxyisopropyl) benzene] was employed

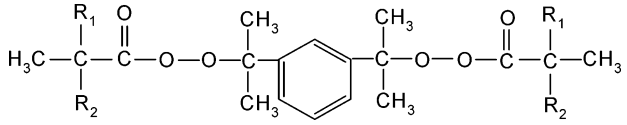

In Table 1, the various molecular species present in the free-radical polymerization of vinyl chloride are shown. These include four types of live polymer chains, five types of inactive polymer chains, and one type of dead polymer chains. As can be seen, the live polymer chains Q_n and S_n contain one undecomposed peroxide group that can undergo further decomposition during the polymerization. All five types of inactive polymer chains (i.e., U_n, V_n, W_n, U'_n, and V'_n) contain at least one undecomposed peroxide group. As a result, these inactive polymeric species can also be reactivated via the decomposition of the terminal peroxide group(s). In other words, there is a sequential production of radicals not only via the decomposition of the bifunctional initiator molecules that commonly occurs with monofunctional initiators but also via the reactivation of the various live and inactive polymer chains throughout the polymerization.

Taking into account the above initiator decomposition and chain reinitiation mechanisms, the following kinetic scheme was postulated for the heterogeneous free-radical polymerization of VC initiated by a mixture of monofunctional (I_m) and bifunctional (I_b) initiators. It should be pointed out that the various elementary reactions are assumed to occur simultaneously in the two phases [i.e., the monomer-rich phase ($j = 1$) and the polymer-rich phase ($j = 2$)].

Decomposition of Monofunctional Initiators

$$I^j_{m,i} \xrightarrow{k^j_{d,i}} 2R^j, \quad i = 1, 2, ..., N_m$$

Decomposition of an Unsymmetrical Bifunctional Initiator

$$I^j_b \xrightarrow{k^j_{dA}} R^j_B + R^j$$

$$I^j_b \xrightarrow{k^j_{dB}} R^j_A + R^j$$

$$R^j_A \xrightarrow{k^j_{dA}} R^j + R'^j$$

$$R^j_B \xrightarrow{k^j_{dB}} R^j + R'^j$$

Chain Initiation

$$R^j + M^j \xrightarrow{k^j_I} P^j_1$$

$$R^j_A + M^j \xrightarrow{k^j_I} Q^j_1$$

$$R^j_B + M^j \xrightarrow{k^j_I} S^j_1$$

$$R'^j + M^j \xrightarrow{2k^j_I} T^j_1$$

Reinitiation of Live and Dead Polymer Chains

$$Q^j_n \xrightarrow{k^j_{dA}} R^j + T^j_n$$

$$S^j_n \xrightarrow{k^j_{dB}} R^j + T^j_n$$

$$U_n \xrightarrow{k^2_{dA}} R^2 + P^2_n$$

$$V_n \xrightarrow{k^2_{dB}} R^2 + P^2_n$$

$$W_n \xrightarrow{k^2_{dA}} R^2 + S^2_n$$

$$W_n \xrightarrow{k^2_{dB}} R^2 + Q^2_n$$

$$U'_n \xrightarrow{2k^2_{dA}} R^2 + Q^2_n$$

$$V'_n \xrightarrow{2k^2_{dB}} R^2 + S^2_n$$

Chain Propagation

$$P^j_n + M^j \xrightarrow{k^j_p} P^j_{n+1}$$

$$Q^j_n + M^j \xrightarrow{k^j_p} Q^j_{n+1}$$

$$S^j_n + M^j \xrightarrow{k^j_p} S^j_{n+1}$$

$$T^j_n + M^j \xrightarrow{2k^j_p} T^j_{n+1}$$

Chain Transfer to Monomer

$$P_n^j + M^j \xrightarrow{k_{fm}^j} D_n + P_1^j$$

$$Q_n^j + M^j \xrightarrow{k_{fm}^j} U_n + P_1^j$$

$$S_n^j + M^j \xrightarrow{k_{fm}^j} V_n + P_1^j$$

$$T_n^j + M^j \xrightarrow{2k_{fm}^j} P_n^j + P_1^j$$

Intramolecular Transfer (Backbiting)

$$P_n^j \xrightarrow{k_b^j} P_n^j$$

$$S_n^j \xrightarrow{k_b^j} S_n^j$$

$$Q_n^j \xrightarrow{k_b^j} Q_n^j$$

$$T_n^j \xrightarrow{2k_b^j} T_n^j$$

Termination by Combination

$$P_n^j + P_m^j \xrightarrow{k_{tc}^j} D_{n+m}$$

$$P_n^j + Q_m^j \xrightarrow{k_{tc}^j} U_{n+m}$$

$$P_n^j + S_m^j \xrightarrow{k_{tc}^j} V_{n+m}$$

$$P_n^j + T_m^j \xrightarrow{2k_{tc}^j} P_{n+m}^j$$

$$Q_n^j + Q_m^j \xrightarrow{k_{tc}^j} U'_{n+m}$$

$$Q_n^j + S_m^j \xrightarrow{k_{tc}^j} W_{n+m}$$

$$Q_n^j + T_m^j \xrightarrow{2k_{tc}^j} Q_{n+m}^j$$

$$S_n^j + S_m^j \xrightarrow{k_{tc}^j} V'_{n+m}$$

$$S_n^j + T_m^j \xrightarrow{2k_{tc}^j} S_{n+m}^j$$

$$T_n^j + T_m^j \xrightarrow{4k_{tc}^j} T_{n+m}^j$$

Termination by Disproportionation

$$P_n^j + P_m^j \xrightarrow{k_{td}^j} D_n + D_m$$

$$P_n^j + Q_m^j \xrightarrow{k_{td}^j} D_n + U_m$$

$$P_n^j + S_m^j \xrightarrow{k_{td}^j} D_n + V_m$$

$$P_n^j + T_m^j \xrightarrow{2k_{td}^j} D_n + P_m^j$$

$$Q_n^j + Q_m^j \xrightarrow{k_{td}^j} U_n + U_m$$

$$Q_n^j + S_m^j \xrightarrow{k_{td}^j} U_n + V_m$$

$$Q_n^j + T_m^j \xrightarrow{2k_{td}^j} U_n + P_m^j$$

$$S_n^j + S_m^j \xrightarrow{k_{td}^j} V_n + V_m$$

$$S_n^j + T_m^j \xrightarrow{2k_{td}^j} V_n + P_m^j$$

$$T_n^j + T_m^j \xrightarrow{4k_{td}^j} P_n^j + P_m^j$$

Inhibition of Live Radical Chains

$$P_n^j + Z^j \xrightarrow{k_z^j} D_n + Z^{\bullet j}$$

$$Q_n^j + Z^j \xrightarrow{k_z^j} U_n + Z^{\bullet j}$$

$$S_n^j + Z^j \xrightarrow{k_z^j} V_n + Z^{\bullet j}$$

$$T_n^j + Z^j \xrightarrow{2k_z^j} P_n^j + Z^{\bullet j}$$

$$Z^{\bullet j} + Z^{\bullet j} \xrightarrow{k_z^j} Z^j + \text{inactive products}$$

In the above kinetic scheme, the symbols Z and M denote inhibitor and monomer molecules, respectively. Primary radicals produced by the initiator decomposition and inhibition reactions are denoted by the symbols R and $Z^{\bullet}$, respectively. N_m is the number of monofunctional initiators used in the polymerization. It should be noted that all of the above reactions except for the reinitiation of the inactive polymer species can take place in the monomer ($j = 1$) and/or the polymer phase ($j = 2$). From the postulated kinetic scheme, one can conclude that chain reinitiation reactions occur via the secondary decomposition of peroxide groups (A and B) located at the end(s) of live and inactive polymer chains. For the inactive polymer chains U'_n and V'_n, the corresponding decomposition rate constants are multiplied by a factor of 2 to account for the presence of two identical peroxide groups in the polymer chain. It should be noted that the inactive polymer chains are assumed to be present only in the polymer-rich phase (because of the low solubility of polymer in the monomer). Notice that both dead and inactive polymer chains are produced via chain transfer to monomer reactions. Finally, it can be observed that all of the elementary reactions (i.e., propagation, chain transfer to monomer, termination by combination, termination by disproportionation, and backbiting) involving live polymer chains containing two active radicals per molecule occur twice as fast as those involving live polymer chains having one radical. Finally, the corresponding rate constant for the termination by combination between two T'_n-type diradicals is multiplied by a factor of 4.

Molecular Species and Moment Rate Functions. To simplify the derivation of the general molecular species rate equations describing the net production rates of live, inactive, and dead polymer chains, the following assumptions were made: (i) The polymerization of VCM in the water and vapor phases is negligible. (ii) The heterogeneous polymerization of VCM proceeds in accordance with the three-stage mechanism described in the Introduction of the paper. (iii) No transfer of radicals between the two reactive phases occurs. (iv) The concentrations of monomer, initiator(s), and inhibitor(s) in the four phases (i.e., vapor, aqueous, monomer, and polymer) are assumed to be in thermodynamic equilibrium at all times. (v) All kinetic rate constants are independent of the polymer chain length. (vi) The long chain approximation (LCA) for the VCM holds true. That is, the monomer is exclusively consumed via chain propagation reactions. (vii) Inactive polymer chains are

present only in the polymer-rich phase. (viii) The quasi-steady-state approximation (QSSA) is applied only to the primary radicals. (ix) The decomposition rate constant for peroxide A is the same for all of the species I_b, R_A, Q_n, U_n, W_n, and U'_n. Similarly, the decomposition rate constant for peroxide B is the same for all of the species I_b, R_B, S_n, V_n, W_n, and V'_n. (x) The reactivities of the two peroxide groups are assumed to be equal for symmetrical initiators and unequal for unsymmetrical ones. (xi) The chain transfer to polymer kinetic rate constant, which has a very small value, is assumed to be negligible.

According to the postulated kinetic scheme and the above assumptions, the net production rates of live, inactive, and dead polymer chains of length n can be derived by combining the formation/consumption rates of the relevant molecular species in the various elementary reactions. In the equations below, note that the concentration of each species is denoted by the italicized species symbol, e.g., P^j_n represents the concentration of live polymer chains of length n in phase j.

Net Production Rates of Live Polymer Chains of Length n

$$\frac{1}{V^j}\frac{d(P^j_n V^j)}{dt} = (k^j_p R^j M^j + k^j_{fm} M^j \sum_{m=1}^{\infty} P^j_m + k^j_{fm} M^j \sum_{m=1}^{\infty} Q^j_m + k^j_{fm} M^j \sum_{m=1}^{\infty} S^j_m)\delta(n-1) + 2k^j_{fm} M^j \sum_{m=1}^{\infty} T^j_m \delta(n-1) + f_{ir} k_{dA}{}^2 U_n \frac{V}{V^j}(j-1) + f_{ir} k_{dB}{}^2 V_n \frac{V}{V^j}(j-1) + k^j_p M^j (P^j_{n-1} - P^j_n) - k^j_{fm} M^j P^j_n + 2k^j_{fm} M^j T - k^j_{tc} P^j_n (\sum_{m=1}^{\infty} P^j_m + \sum_{m=1}^{\infty} Q^j_m + \sum_{m=1}^{\infty} S^j_m + 2\sum_{m=1}^{\infty} T^j_m) + 2k^j_{tc} \sum_{m=1}^{n-1} P^j_m T^j_{n-m} - k^j_{td} P^j_n (\sum_{m=1}^{\infty} P^j_m + \sum_{m=1}^{\infty} Q^j_m + \sum_{m=1}^{\infty} S^j_m + 2\sum_{m=1}^{\infty} T^j_m) + 2k^j_{td} T^j_n (\sum_{m=1}^{\infty} P^j_m + \sum_{m=1}^{\infty} Q^j_m + \sum_{m=1}^{\infty} S^j_m + 2\sum_{m=1}^{\infty} T^j_m) - k^j_z Z^j P^j_n + 2k^j_z Z^j T^j_n + (1 - f_{ir})(k^j_{dA} Q^j_n + k^j_{dB} S^j_n) \quad (26)$$

$$\frac{1}{V^j}\frac{d(Q^j_n V^j)}{dt} = k^j_p M^j R^j_A \delta(n-1) - k^j_{dA} Q^j_n + f_{ir} k_{dB}{}^2 W_n \frac{V}{V^j}(j-1) + 2f_{ir} k_{dA}{}^2 U'_n \frac{V}{V^j}(j-1) + k^j_p M^j (Q^j_{n-1} - Q^j_n) - k^j_{fm} M^j Q^j_n - k^j_{tc} Q^j_n (\sum_{m=1}^{\infty} P^j_m + \sum_{m=1}^{\infty} Q^j_m + \sum_{m=1}^{\infty} S^j_m + 2\sum_{m=1}^{\infty} T^j_m) + 2k^j_{tc} \sum_{m=1}^{n-1} Q^j_m T^j_{n-m} - k^j_{td} Q^j_n (\sum_{m=1}^{\infty} P^j_m + \sum_{m=1}^{\infty} Q^j_m + \sum_{m=1}^{\infty} S^j_m + 2\sum_{m=1}^{\infty} T^j_m) - k^j_z Z^j Q^j_n \quad (27)$$

$$\frac{1}{V^j}\frac{d(S^j_n V^j)}{dt} = k^j_p M^j R^j_B \delta(n-1) - k^j_{dB} S^j_n + f_{ir} k_{dA}{}^2 W_n \frac{V}{V^j}(j-1) + 2f_{ir} k_{dB}{}^2 V'_n \frac{V}{V^j}(j-1) + k^j_p M^j (S^j_{n-1} - S^j_n) - k^j_{fm} M^j S^j_n - k^j_{tc} S^j_n (\sum_{m=1}^{\infty} P^j_m + \sum_{m=1}^{\infty} Q^j_m + \sum_{m=1}^{\infty} S^j_m + 2\sum_{m=1}^{\infty} T^j_m) + 2k^j_{tc} \sum_{m=1}^{n-1} S^j_m T^j_{n-m} - k^j_{td} S^j_n (\sum_{m=1}^{\infty} P^j_m + \sum_{m=1}^{\infty} Q^j_m + \sum_{m=1}^{\infty} S^j_m + 2\sum_{m=1}^{\infty} T^j_m) - k^j_z Z^j S^j_n \quad (28)$$

$$\frac{1}{V^j}\frac{d(T^j_n V^j)}{dt} = 2k^j_p M^j R'^j \delta(n-1) + f_{ir} k^j_{dA} Q^j_n + f_{ir} k^j_{dB} S^j_n + 2k^j_p M^j (T^j_{n-1} - T^j_n) - 2k^j_{fm} M^j T^j_n - 2k^j_{tc} T^j_n (\sum_{m=1}^{\infty} P^j_m + \sum_{m=1}^{\infty} Q^j_m + \sum_{m=1}^{\infty} S^j_m + 2\sum_{m=1}^{\infty} T^j_m) + 2k^j_{tc} \sum_{m=1}^{n-1} T^j_m T^j_{n-m} - 2k^j_{td} T^j_n (\sum_{m=1}^{\infty} P^j_m + \sum_{m=1}^{\infty} Q^j_m + \sum_{m=1}^{\infty} S^j_m + 2\sum_{m=1}^{\infty} T^j_m) - 2k^j_z Z^j T^j_n \quad (29)$$

Net Production Rates of Inactive Polymer Chains of Length n

$$\frac{1}{V}\frac{d(U_n V)}{dt} = -k_{dA}{}^2 U_n + \sum_{j=1}^{2} k^j_{fm} M^j Q^j_n \frac{V^j}{V} + \sum_{j=1}^{2} k^j_{tc} \sum_{m=1}^{n-1} P^j_m Q^j_{n-m} \frac{V^j}{V} + \sum_{j=1}^{2} k^j_{td} Q^j_n (\sum_{m=1}^{\infty} P^j_m + \sum_{m=1}^{\infty} Q^j_m + \sum_{m=1}^{\infty} S^j_m + 2\sum_{m=1}^{\infty} T^j_m) \frac{V^j}{V} + \sum_{j=1}^{2} k^j_z Z^j Q^j_n \frac{V^j}{V} + (1 - f_{ir})(k_{dB}{}^2 W_n + 2k_{dA}{}^2 U'_n) \quad (30)$$

$$\frac{1}{V}\frac{d(V_n V)}{dt} = -k_{dB}{}^2 V_n + \sum_{j=1}^{2} k^j_{fm} M^j S^j_n \frac{V^j}{V} + \sum_{j=1}^{2} k^j_{tc} \sum_{m=1}^{n-1} P^j_m S^j_{n-m} \frac{V^j}{V} + \sum_{j=1}^{2} k^j_{td} S^j_n (\sum_{m=1}^{\infty} P^j_m + \sum_{m=1}^{\infty} Q^j_m + \sum_{m=1}^{\infty} S^j_m + 2\sum_{m=1}^{\infty} T^j_m) \frac{V^j}{V} + \sum_{j=1}^{2} k^j_z Z^j S^j_n \frac{V^j}{V} + (1 - f_{ir})(k_{dA}{}^2 W_n + 2k_{dB}{}^2 V'_n) \quad (31)$$

$$\frac{1}{V}\frac{d(W_n V)}{dt} = -(k_{dA}{}^2 + k_{dB}{}^2) W_n + \sum_{j=1}^{2} k_{tc}{}^2 \sum_{m=1}^{n-1} Q^j_m S^j_{n-m} \frac{V^j}{V} \quad (32)$$

$$\frac{1}{V}\frac{d(U'_n V)}{dt} = -2k_{dA}{}^2 U'_n + \frac{1}{2}\sum_{j=1}^{2} k^j_{tc} \sum_{m=1}^{n-1} Q^j_m Q^j_{n-m} \frac{V^j}{V} \quad (33)$$

$$\frac{1}{V}\frac{d(V'_n V)}{dt} = -2k_{dB}{}^2 V'_n + \frac{1}{2}\sum_{j=1}^{2} k^j_{tc} \sum_{m=1}^{n-1} S^j_m S^j_{n-m} \frac{V^j}{V} \quad (34)$$

Net Production Rate of Dead Polymer Chains of Length n

$$\frac{1}{V}\frac{\mathrm{d}(\mathrm{D}_n V)}{\mathrm{d}t} = \sum_{j=1}^{2} k_{\mathrm{fm}}^{j} M^{j} P_n^{j} \frac{V^j}{V} + \frac{1}{2}\sum_{j=1}^{2} k_{\mathrm{tc}}^{j} \sum_{m=1}^{n-1} P_m^{j} P_{n-m}^{j} \frac{V^j}{V} + \sum_{j=1}^{2} k_{\mathrm{td}}^{j} P_n^{j} \left(\sum_{m=1}^{\infty} P_m^{j} + \sum_{m=1}^{\infty} Q_m^{j} + \sum_{m=1}^{\infty} S_m^{j} + 2\sum_{m=1}^{\infty} T_m^{j}\right)\frac{V^j}{V} + \sum_{j=1}^{2} k_{\mathrm{z}}^{j} Z^{j} P_n^{j} \frac{V^j}{V} + (1 - f_{\mathrm{ir}})(k_{\mathrm{dA}}{}^2 U_n + k_{\mathrm{dB}}{}^2 V_n) \quad (35)$$

where $\delta(n-1)$ is the Kronecker delta [i.e., $\delta(n-1)$ equals 1 for $n = 1$ and 0 for $n \neq 1$].

Moment Rate Functions. Application of the fundamental mass conservation equations to the various molecular species present in a batch reactor (e.g., live, inactive, and dead polymer chains of various lengths) typically results in an infinite system of differential equations. To reduce the high dimensionality of the numerical problem, several mathematical techniques have been proposed in the literature.[32] In the present study, the method of moments was utilized to recast the "infinite" system of dynamic molar species balance equations into a low-order system of differential moment equations that can easily be solved. The method of moments is based on the statistical representation of the average molecular properties of the polymer in terms of the leading moments of the number chain length distributions (NCLDs) of the live, inactive, and dead polymer chains. Accordingly, one can define the following moments for the various (NCLDs) present in the heterophase polymerization system

$$\lambda_{\xi,k}^{j} = \sum_{n=i}^{\infty} n^{k} \xi_n^{j}, \quad \xi = \mathrm{P, Q, S, T}; j = 1, 2 \quad (36)$$

$$\lambda_{\theta,k} = \sum_{n=i}^{\infty} n^{k} \theta_n, \quad \theta = \mathrm{U, V, W, U', V'} \quad (37)$$

$$\mu_k = \sum_{n=i}^{\infty} n^{k} \mathrm{D}_n \quad (38)$$

where $\lambda_{\xi,k}^{j}$ denotes the kth moment of polymer species ξ in phase j. Similarly, $\lambda_{\theta,k}$ is the kth moment of polymer species θ in the polymer-rich phase, and μ_k is the kth moment of dead polymer chains D_n in the polymer-rich phase.

The rate functions for moments $\lambda_{\xi,k}^{j}$, $\lambda_{\theta,k}$, and μ_k can be obtained from eqs 26−35 by multiplying each term by n^k and summing the resulting expressions over the total range of n. The final equations for the relevant moment rate functions are as follows:

Live Polymer Moment Rate Equations

$$r_{\lambda_{\mathrm{P},k}^{j}} = k_{\mathrm{p}}^{j} R^{j} M^{j} + f_{\mathrm{ir}} k_{\mathrm{dA}}{}^2 \lambda_{\mathrm{U},k} \frac{V}{V^2}(j-1) + f_{\mathrm{ir}} k_{\mathrm{dB}}{}^2 \lambda_{\mathrm{V},k} \frac{V}{V^2}(j-1) + k_{\mathrm{p}}^{j} M^{j}\left[\sum_{r=0}^{k}\binom{k}{r}\lambda_{\mathrm{P},r}^{j} - \lambda_{\mathrm{P},k}^{j}\right] + k_{\mathrm{fm}}^{j} M^{j}(\lambda_{\mathrm{P},0}^{j} + \lambda_{\mathrm{Q},0}^{j} + \lambda_{\mathrm{S},0}^{j} + 2\lambda_{\mathrm{T},0}^{j}) - k_{\mathrm{fm}}^{j} M^{j}(\lambda_{\mathrm{P},k}^{j} - 2\lambda_{\mathrm{T},k}^{j}) - k_{\mathrm{tc}}^{j} \lambda_{\mathrm{P},k}^{j}(\lambda_{\mathrm{P},0}^{j} + \lambda_{\mathrm{Q},0}^{j} + \lambda_{\mathrm{S},0}^{j} + 2\lambda_{\mathrm{T},0}^{j}) + 2k_{\mathrm{tc}}^{j}\left[\sum_{r=0}^{k}\binom{k}{r}\lambda_{\mathrm{P},r}^{j}\lambda_{\mathrm{T},k-r}^{j}\right] - k_{\mathrm{td}}^{j}\lambda_{\mathrm{P},k}^{j}(\lambda_{\mathrm{P},0}^{j} + \lambda_{\mathrm{Q},0}^{j} + \lambda_{\mathrm{S},0}^{j} + 2\lambda_{\mathrm{T},0}^{j}) + 2k_{\mathrm{td}}^{j}\lambda_{\mathrm{T},k}^{j}(\lambda_{\mathrm{P},0}^{j} + \lambda_{\mathrm{Q},0}^{j} + \lambda_{\mathrm{S},0}^{j} + 2\lambda_{\mathrm{T},0}^{j}) - k_{\mathrm{z}}^{j} Z^{j}\lambda_{\mathrm{P},k}^{j} + 2k_{\mathrm{z}}^{j} Z^{j}\lambda_{\mathrm{T},k}^{j} + (1 - f_{\mathrm{ir}})(k_{\mathrm{dA}}^{j}\lambda_{\mathrm{Q},k}^{j} + k_{\mathrm{dB}}^{j}\lambda_{\mathrm{S},k}^{j}) \quad (39)$$

$$r_{\lambda_{\mathrm{Q},k}^{j}} = k_{\mathrm{p}}^{j} R_{\mathrm{A}}^{j} M^{j} - k_{\mathrm{dA}}^{j}\lambda_{\mathrm{Q},k}^{j} + f_{\mathrm{ir}} k_{\mathrm{dB}}{}^2 \lambda_{\mathrm{W},k} \frac{V}{V^2}(j-1) + k_{\mathrm{p}}^{j} M^{j}\left[\sum_{r=0}^{k}\binom{k}{r}\lambda_{\mathrm{Q},r}^{j} - \lambda_{\mathrm{Q},k}^{j}\right] + 2f_{\mathrm{ir}} k_{\mathrm{dA}}{}^2 \lambda_{\mathrm{U}',k} \frac{V}{V^2}(j-1) - k_{\mathrm{fm}}^{j} M^{j}\lambda_{\mathrm{Q},k}^{j} - k_{\mathrm{tc}}^{j}\lambda_{\mathrm{Q},k}^{j}(\lambda_{\mathrm{P},0}^{j} + \lambda_{\mathrm{Q},0}^{j} + \lambda_{\mathrm{S},0}^{j} + 2\lambda_{\mathrm{T},0}^{j}) + 2k_{\mathrm{tc}}^{j}\left[\sum_{r=0}^{k}\binom{k}{r}\lambda_{\mathrm{Q},r}^{j}\lambda_{\mathrm{T},k-r}^{j}\right] - k_{\mathrm{td}}^{j}\lambda_{\mathrm{Q},k}^{j}(\lambda_{\mathrm{P},0}^{j} + \lambda_{\mathrm{Q},0}^{j} + \lambda_{\mathrm{S},0}^{j} + 2\lambda_{\mathrm{T},0}^{j}) - k_{\mathrm{z}}^{j} Z^{j}\lambda_{\mathrm{Q},k}^{j} \quad (40)$$

$$r_{\lambda_{\mathrm{S},k}^{j}} = k_{\mathrm{p}}^{j} R_{\mathrm{B}}^{j} M^{j} - k_{\mathrm{dB}}^{j}\lambda_{\mathrm{S},k}^{j} + f_{\mathrm{ir}} k_{\mathrm{dA}}{}^2 \lambda_{\mathrm{W},k} \frac{V}{V^2}(j-1) + k_{\mathrm{p}}^{j} M^{j}\left[\sum_{r=0}^{k}\binom{k}{r}\lambda_{\mathrm{S},r}^{j} - \lambda_{\mathrm{S},k}^{j}\right] + 2f_{\mathrm{ir}} k_{\mathrm{dB}}{}^2 \lambda_{\mathrm{V}',k} \frac{V}{V^2}(j-1) - k_{\mathrm{fm}}^{j} M^{j}\lambda_{\mathrm{S},k}^{j} - k_{\mathrm{tc}}^{j}\lambda_{\mathrm{S},k}^{j}(\lambda_{\mathrm{P},0}^{j} + \lambda_{\mathrm{Q},0}^{j} + \lambda_{\mathrm{S},0}^{j} + 2\lambda_{\mathrm{T},0}^{j}) + 2k_{\mathrm{tc}}^{j}\left[\sum_{r=0}^{k}\binom{k}{r}\lambda_{\mathrm{S},r}^{j}\lambda_{\mathrm{T},k-r}^{j}\right] - k_{\mathrm{td}}^{j}\lambda_{\mathrm{S},k}^{j}(\lambda_{\mathrm{P},0}^{j} + \lambda_{\mathrm{Q},0}^{j} + \lambda_{\mathrm{S},0}^{j} + 2\lambda_{\mathrm{T},0}^{j}) - k_{\mathrm{z}}^{j} Z^{j}\lambda_{\mathrm{S},k}^{j} \quad (41)$$

$$r_{\lambda_{\mathrm{T},k}^{j}} = 2k_{\mathrm{p}}^{j} R'^{j} M^{j} + f_{\mathrm{ir}} k_{\mathrm{dA}}^{j}\lambda_{\mathrm{Q},k}^{j} + f_{\mathrm{ir}} k_{\mathrm{dB}}^{j}\lambda_{\mathrm{S},k}^{j} + 2k_{\mathrm{p}}^{j}\left[\sum_{r=0}^{k}\binom{k}{r}\lambda_{\mathrm{T},r}^{j} - \lambda_{\mathrm{T},k}^{j}\right] - 2k_{\mathrm{fm}}^{j} M^{j}\lambda_{\mathrm{T},k}^{j} - 2k_{\mathrm{tc}}^{j}\lambda_{\mathrm{T},k}^{j}(\lambda_{\mathrm{P},0}^{j} + \lambda_{\mathrm{Q},0}^{j} + \lambda_{\mathrm{S},0}^{j} + 2\lambda_{\mathrm{T},0}^{j}) + 2k_{\mathrm{tc}}^{j}\left[\sum_{r=0}^{k}\binom{k}{r}\lambda_{\mathrm{T},r}^{j}\lambda_{\mathrm{T},k-r}^{j}\right] - 2k_{\mathrm{td}}^{j}\lambda_{\mathrm{T},k}^{j}(\lambda_{\mathrm{P},0}^{j} + \lambda_{\mathrm{Q},0}^{j} + \lambda_{\mathrm{S},0}^{j} + 2\lambda_{\mathrm{T},0}^{j}) - 2k_{\mathrm{z}}^{j} Z^{j}\lambda_{\mathrm{T},k}^{j} \quad (42)$$

Inactive Polymer Moment Rate Equations

$$r_{\lambda_{\mathrm{U},k}} = -k_{\mathrm{dA}}{}^2\lambda_{\mathrm{U},k} + \sum_{j=1}^{2} k_{\mathrm{fm}}^{j} M^{j}\lambda_{\mathrm{Q},k}^{j}\frac{V^j}{V} + \sum_{j=1}^{2} k_{\mathrm{tc}}^{j}\left[\sum_{r=0}^{k}\binom{k}{r}\lambda_{\mathrm{P},r}^{j}\lambda_{\mathrm{Q},k-r}^{j}\right]\frac{V^j}{V} + \sum_{j=1}^{2} k_{\mathrm{td}}^{j}\lambda_{\mathrm{Q},k}^{j}(\lambda_{\mathrm{P},0}^{j} + \lambda_{\mathrm{Q},0}^{j} + \lambda_{\mathrm{S},0}^{j} + 2\lambda_{\mathrm{T},0}^{j}) + \sum_{j=1}^{2} k_{\mathrm{z}}^{j} Z^{j}\lambda_{\mathrm{Q},k}^{j}\frac{V^j}{V} + (1 - f_{\mathrm{ir}})(k_{\mathrm{dB}}{}^2\lambda_{\mathrm{W},k} + 2k_{\mathrm{dA}}{}^2\lambda_{\mathrm{U}',k}) \quad (43)$$

$$r_{\lambda_{\mathrm{V},k}} = -k_{\mathrm{dB}}{}^2\lambda_{\mathrm{V},k} + \sum_{j=1}^{2} k_{\mathrm{fm}}^{j} M^{j}\lambda_{\mathrm{S},k}^{j}\frac{V^j}{V} + \sum_{j=1}^{2} k_{\mathrm{tc}}^{j}\left[\sum_{r=0}^{k}\binom{k}{r}\lambda_{\mathrm{P},r}^{j}\lambda_{\mathrm{S},k-r}^{j}\right]\frac{V^j}{V} + \sum_{j=1}^{2} k_{\mathrm{td}}^{j}\lambda_{\mathrm{S},k}^{j}(\lambda_{\mathrm{P},0}^{j} + \lambda_{\mathrm{Q},0}^{j} + \lambda_{\mathrm{S},0}^{j} + 2\lambda_{\mathrm{T},0}^{j}) + \sum_{j=1}^{2} k_{\mathrm{z}}^{j} Z^{j}\lambda_{\mathrm{S},k}^{j}\frac{V^j}{V} + (1 - f_{\mathrm{ir}})(k_{\mathrm{dA}}{}^2\lambda_{\mathrm{W},k} + 2k_{\mathrm{dB}}{}^2\lambda_{\mathrm{V}',k}) \quad (44)$$

$$r_{\lambda_{\mathrm{W},k}} = -(k_{\mathrm{dB}}{}^2 + k_{\mathrm{dA}}{}^2)\lambda_{\mathrm{W},k} + \sum_{j=1}^{2} k_{\mathrm{tc}}^{j}\left[\sum_{r=0}^{k}\binom{k}{r}\lambda_{\mathrm{Q},r}^{j}\lambda_{\mathrm{S},k-r}^{j}\right]\frac{V^j}{V} \quad (45)$$

$$r_{\lambda_{\mathrm{U}',k}} = -2k_{\mathrm{dA}}{}^2\lambda_{\mathrm{U}',k} + \frac{1}{2}\sum_{j=1}^{2} k_{\mathrm{tc}}^{j}\left[\sum_{r=0}^{k}\binom{k}{r}\lambda_{\mathrm{Q},r}^{j}\lambda_{\mathrm{Q},k-r}^{j}\right]\frac{V^j}{V} \quad (46)$$

$$r_{\lambda_{V',k}} = -2k_{dB}{}^2\lambda_{V',k} + \frac{1}{2}\sum_{j=1}^{2}k_{tc}^{j}\left[\sum_{r=0}^{k}\binom{k}{r}\lambda_{S,r}^{j}\lambda_{S,k-r}^{j}\right]\frac{V^j}{V} \quad (47)$$

Dead Polymer Moment Rate Equation

$$r_{\mu_k} = \sum_{j=1}^{2}k_{fm}^{j}M^{j}\lambda_{P,k}^{j}\frac{V^j}{V} + \frac{1}{2}\sum_{j=1}^{2}k_{tc}^{j}\sum_{r=0}^{k}\binom{k}{r}\lambda_{P,r}^{j}\lambda_{P,k-r}^{j}\frac{V^j}{V} + \sum_{j=1}^{2}k_{td}^{j}\lambda_{P,k}^{j}(\lambda_{P,0}^{j} + \lambda_{Q,0}^{j} + \lambda_{S,0}^{j} + 2\lambda_{T,0}^{j})\frac{V^j}{V} + \sum_{j=1}^{2}k_{z}^{j}Z^{j}\lambda_{P,k}^{j}\frac{V^j}{V} + (1 - f_{ir})(k_{dA}{}^2\lambda_{U,k} + k_{dB}{}^2\lambda_{V,k}) \quad (48)$$

Accordingly, the number- and weight-average molecular weights can easily be calculated in terms of the leading moments of the live, inactive, and dead NCLDs

Number-Average Molecular Weight

$$M_n = (\mu_1 + \lambda_{U,1} + \lambda_{V,1} + \lambda_{W,1} + \lambda_{U',1} + \lambda_{V',1} + \lambda_{P,1}^{1} + \lambda_{S,1}^{1} + \lambda_{Q,1}^{1} + \lambda_{T,1}^{1} + \lambda_{P,1}^{2} + \lambda_{S,1}^{2} + \lambda_{Q,1}^{2} + \lambda_{T,1}^{2})/(\mu_0 + \lambda_{U,0} + \lambda_{V,0} + \lambda_{W,0} + \lambda_{U',0} + \lambda_{V',0} + \lambda_{P,0}^{1} + \lambda_{S,0}^{1} + \lambda_{Q,0}^{1} + \lambda_{T,0}^{1} + \lambda_{P,0}^{2} + \lambda_{S,0}^{2} + \lambda_{Q,0}^{2} + \lambda_{T,0}^{2})MW_m \quad (49)$$

Weight-Average Molecular Weight

$$M_w = (\mu_2 + \lambda_{U,2} + \lambda_{V,2} + \lambda_{W,2} + \lambda_{U',2} + \lambda_{V',2} + \lambda_{P,2}^{1} + \lambda_{S,2}^{1} + \lambda_{Q,2}^{1} + \lambda_{T,2}^{1} + \lambda_{P,2}^{2} + \lambda_{S,2}^{2} + \lambda_{Q,2}^{2} + \lambda_{T,2}^{2})/(\mu_1 + \lambda_{U,1} + \lambda_{V,1} + \lambda_{W,1} + \lambda_{U',1} + \lambda_{V',1} + \lambda_{P,1}^{1} + \lambda_{S,1}^{1} + \lambda_{Q,1}^{1} + \lambda_{T,1}^{1} + \lambda_{P,1}^{2} + \lambda_{S,1}^{2} + \lambda_{Q,1}^{2} + \lambda_{T,1}^{2})MW_m \quad (50)$$

The polydispersity index (PD), which is a measure of the broadness of the molecular weight distribution, is given by the ratio of the weight-average molecular weight to the number-average molecular weight (i.e., $PD = M_w/M_n$).

With the general kinetic scheme postulated in this study, two additional structural characteristics of the polymer chains can be identified. These are the concentration of short chain branches (SCB) per molecule and the concentration of terminal double bonds (TDB) per molecule. To calculate the time variation of these molecular properties, the following differential equations need to be considered as well

$$\frac{d(SCB)}{dt} = \sum_{j=1}^{2}k_{b}^{j}(\lambda_{P,0}^{j} + \lambda_{S,0}^{j} + \lambda_{Q,0}^{j} + 2\lambda_{T,0}^{j}) \quad (51)$$

$$\frac{d(TDB)}{dt} = \sum_{j=1}^{2}[k_{fm}^{j}M^{j}(\lambda_{P,0}^{j} + \lambda_{S,0}^{j} + \lambda_{Q,0}^{j} + 2\lambda_{T,0}^{j}) + k_{td}^{j}(\lambda_{P,0}^{j} + \lambda_{S,0}^{j} + \lambda_{Q,0}^{j} + 2\lambda_{T,0}^{j})^2] \quad (52)$$

Reactor Design Equations and Phase Equilibrium Calculation

Using the above definitions of the moment rate functions and the net production/consumption rates of all species of interest (in terms of the concentrations of monofunctional and bifunctional initiators, the concentration of primary radicals, the total monomer conversion, etc.), the design equations for a batch polymerization reactor can easily be derived as follows:

Monofunctional Initiator(s)

$$\frac{1}{V}\frac{d(VI_{m,i})}{dt} = \sum_{j=1}^{2} - k_{d,i}^{j}I_{m,i}^{j}, \quad i = 1, 2, ..., N_m \quad (53)$$

Bifunctional Initiator

$$\frac{1}{V}\frac{d(VI_b)}{dt} = \sum_{j=1}^{2} - (k_{dA}^{j} + k_{dB}^{j})I_b^j \quad (54)$$

Primary Radicals R

$$\frac{1}{V^j}\frac{d(R^jV^j)}{dt} = \sum_{i=1}^{N_m}2f_ik_{d,i}^{j}I_{m,i}^{j} + f_{bR}k_{dA}^{j}I_b^j + f_{bR}k_{dB}^{j}I_b^j + f_{bR}k_{dA}^{j}R_A^j + f_{bR}k_{dB}^{j}R_B^j - k_p^jM^jR^j + f_{bR}k_{dA}^{j}\sum_{n=1}^{\infty}Q_n^j + f_{bR}k_{dB}^{j}\sum_{n=1}^{\infty}S_n^j + \left(f_{bR}k_{dA}{}^2\sum_{n=1}^{\infty}(U_n + W_n + 2U_n')\frac{V}{V^2} + f_{bR}k_{dB}{}^2\sum_{n=1}^{\infty}(V_n + W_n + 2V_n')\frac{V}{V^2}\right)(j-1) \quad (55)$$

Primary Radicals R_A

$$\frac{1}{V^j}\frac{d(R_A^jV^j)}{dt} = f_{bA}k_{dB}^{j}I_b^j - k_{dA}^{j}R_A^j - k_p^jR_A^jM^j \quad (56)$$

Primary Radicals R_B

$$\frac{1}{V^j}\frac{d(R_B^jV^j)}{dt} = f_{bB}k_{dA}^{j}I_b^j - k_{dB}^{j}R_B^j - k_p^jR_B^jM^j \quad (57)$$

Primary Diradicals R′

$$\frac{1}{V^j}\frac{d(R'^jV^j)}{dt} = f_{bR'}k_{dA}^{j}R_A^j + f_{bR'}k_{dB}^{j}R_B^j - 2k_p^jM^jR'^j \quad (58)$$

Inhibitor

$$\frac{1}{V}\frac{d(ZV)}{dt} = \sum_{j=1}^{2} - [k_z^jZ^j(\lambda_{P,0}^{j} + \lambda_{S,0}^{j} + \lambda_{Q,0}^{j} + 2\lambda_{T,0}^{j})] \quad (59)$$

Total Monomer Conversion

$$\frac{dX}{dt} = \sum_{j=1}^{2}k_p^j\frac{M^j}{M_0}(\lambda_{P,0}^{j} + \lambda_{S,0}^{j} + \lambda_{Q,0}^{j} + 2\lambda_{T,0}^{j}) \quad (60)$$

Live, Inactive, and Dead Moments

$$\frac{1}{V^j}\frac{d(V^j\lambda_{\xi,k}^{j})}{dt} = r_{\lambda_{\xi,k}^{j}}, \quad j = 1, 2 \quad (61)$$

$$\frac{1}{V^2}\frac{d(V^2\lambda_{\theta,k}{}^2)}{dt} = r_{\lambda_{\theta,k}^2} \quad (62)$$

$$\frac{1}{V^2}\frac{d(V^2\mu_k{}^2)}{dt} = r_{\mu_k^2} \quad (63)$$

where f_i is the initiator efficiency of monofunctional initiator i. f_{bR} is the fraction of the R type of primary radicals (i.e., those formed via the decomposition of the bifunctional initiator) leading to the formation of new polymer chains. f_{bA} and f_{bB} are the respective efficiencies of the R_A and R_B primary radicals, and $f_{bR'}$ is the fraction

of R′ diradical species leading to initiation of new polymer chains. For simplification, the efficiencies f_{bA}, f_{bB}, and $f_{bR'}$ are assumed to be equal. Finally, f_{ir} denotes the corresponding fraction of new macroradicals formed via the decomposition of the molecular species Q_n, S_n, U_n, U'_n, V_n, V'_n and W_n.

Phase Equilibrium Calculations. The vapor phase that occupies the free space on top of the liquid mixture in the reactor consists mainly of VCM and water vapors. When a separate liquid monomer phase exists (i.e., in the conversion range $0 < X < X_f$), the reactor pressure will be equal to the sum of the VCM and water partial pressures. It should be noted that a small amount of residual air might be present in the overhead vapor phase. However, because of the very low vacuum (i.e., less than 0.1 bar) typically applied to an industrial reactor before its loading, the amount of air in the overhead vapor phase can be assumed to be negligible in the reactor pressure calculation. In stage II of VCM polymerization, the polymer-rich phase remains saturated with monomer, reflecting the thermodynamic equilibrium between the two phases (i.e., the monomer- and polymer-rich phases). However, upon the disappearance of the separate monomer phase (i.e., at the critical monomer conversion $X = X_f$), the reactor pressure starts to decrease because of the transfer of monomer from the overhead vapor phase to the dispersed monomer-swollen polymer particles.

Throughout the duration of VCM polymerization, the four phases are assumed to be in thermodynamic equilibrium. As a result, the fugacities of VCM in the four phases must be equal

$$\hat{f}^{g}_{m} = \hat{f}^{w}_{m} = \hat{f}^{m}_{m} = \hat{f}^{p}_{m} \tag{64}$$

Following the original developments of Xie et al.[31] and Kiparissides et al.,[23] the fugacity coefficient of VCM, $\hat{\phi}_m$, in the gas phase is given by

$$\ln(\hat{\phi}_m) = \ln\left(\frac{\hat{f}^{g}_{m}}{P_m}\right) = \ln\left(\frac{\hat{f}^{g}_{m}}{y_m P}\right) = \frac{P}{RT}[B_m + (1 - y_m)^2\delta_{mw}] \tag{65}$$

where

$$\delta_{mw} = 2B_{mw} - B_m - B_w \tag{66}$$

P, B_i, and δ_{mw} are the total reactor pressure, the second virial coefficient of the ith component, and the monomer solubility in the aqueous phase, respectively.[23] Assuming that the water vapor partial pressure is equal to its respective saturation value, the mole fraction of VCM in the vapor phase, y_m, can be calculated from the following equation

$$y_m = (1 - y_w) = 1 - P^{sat}_{w}/P \tag{67}$$

The monomer activity, a_m, in the polymer-rich phase will be given by the ratio of the monomer fugacity coefficient in the polymer phase to its corresponding value in the standard state. The latter is assumed to be equal to the fugacity of the pure monomer at the reaction temperature and the respective monomer saturation pressure. According to the Flory−Huggins equation, the monomer activity can be expressed in terms of the polymer volume fraction in the polymer-rich phase, ϕ_2, and the Flory−Huggins interaction parameter, χ^{23}

$$\ln(a_m) = \ln(\hat{f}^{p}_{m}/f^{0}_{m}) = \ln(1 - \phi_2) + \phi_2 + \chi\phi_2^{\,2} \tag{68}$$

From eqs 64, 65, and 68, one can easily obtain the following equation for the calculation of the total reactor pressure, P

$$f^{0}_{m}\exp[\ln(1 - \phi_2) + \phi_2 + \chi\phi_2^{\,2}] = y_m P \exp\left\{\frac{P}{RT}[B_m + (1 - y_m)^2\delta_{mw}]\right\} \tag{69}$$

In the conversion range $0 < X < X_f$, the polymer phase will be saturated with monomer. As a result, the monomer activity, a_m, will be equal to 1. Thus, from eq 68 for $a_m = 1$, the critical value of $\phi_{2,c}$ can be obtained

$$0 = \ln(1 - \phi_{2,c}) + \phi_{2,c} + \chi\phi_{2,c}^{\,2} \tag{70}$$

Calculation of the Monomer Distribution. To calculate the individual polymerization rates in the monomer- and polymer-rich phases, the VCM distribution in the four phases must be known. Assuming that the four phases in the system are in thermodynamic equilibrium throughout, one can easily derive the following pseudo-steady-state monomer mass balance

$$M_0(1 - X) = M_m + M_p + M_a + M_g \tag{71}$$

where the symbols M_0, M_m, M_p, M_a, and M_g denote the total mass of VCM loaded in the reactor and the masses of VCM in the monomer (m), polymer (p), aqueous (a), and gas (g) phases, respectively.

During the first stage ($0 < X < 0.001$), no separate polymer phase exists (i.e., $M_p = 0$). Therefore, the mass of VCM in the monomer-rich phase will be

$$M_m = M_0(1 - X) - M_a - M_g \tag{72}$$

According to Kiparissides et al.,[23] the mass of VCM in the aqueous phase will be given by

$$M_a = K(P/P^{sat}_{m})W_{wa} \tag{73}$$

where K is the VCM solubility in the aqueous phase (i.e., $K = 0.0088$ g of VCM per gram of H_2O)[34] and P^{sat}_{m} is the saturated monomer vapor pressure at the polymerization temperature. The mass of H_2O in the aqueous phase, W_{wa}, is given by the equation

$$W_{wa} = W_w - (\hat{f}^{g}_{w}MW_w V_g/RT) \tag{74}$$

where W_w is the total mass of water loaded in the reactor and V_g is the volume of the gas phase calculated by the following equation

$$V_g = \frac{V_R - \frac{M_0}{\rho_m} - \frac{W_w}{\rho_w} + M_0X(\rho_m^{-1} - \rho_p^{-1})}{1 - (\hat{f}^{g}_{m}MW_m/\rho_m + \hat{f}^{g}_{w}MW_w/\rho_w)/RT} \tag{75}$$

where V_R is the total reactor volume and ρ_m, ρ_p, and ρ_w are the monomer, polymer, and water densities, respectively. The symbol MW_x denotes the molecular weight of molecular species x.

The fugacity of water in the vapor phase, $\hat{f}^{g}_{w}$, will be equal to the total reactor pressure, P, minus the fugacity

of the monomer in the gas phase, $\hat{f}_w^g$, i.e.

$$\hat{f}_w^g = P - \hat{f}_m \tag{76}$$

Accordingly, the mass of VCM in the gas phase can be calculated in terms of its fugacity, $\hat{f}_w^g$; the volume of the gas phase, V_g; and the temperature, T, as

$$M_g = \hat{f}_m^g \mathrm{MW}_m V_g / RT \tag{77}$$

Applying similar considerations, the monomer distribution in the monomer-rich and polymer-rich phases during stage II of the VCM polymerization (i.e., $0.001 < X < X_f$) will be given by the following equations

$$M_m = M_0\left(1 - \frac{X}{X_S}\right) - M_a - M_g \tag{78}$$

$$M_p = M_0 \frac{X}{X_S}(1 - X_S) \tag{79}$$

where

$$X_S = \frac{\phi_{2,c}\rho_p}{\phi_{2,c}\rho_p + (1 - \phi_{2,c})\rho_m} \tag{80}$$

The values of M_a and M_g are calculated from eqs 73 and 77, respectively. During this polymerization stage, the monomer concentrations in the monomer-rich (1) and polymer-rich (2) phases will be given by

$$[M_m] = \rho_m/\mathrm{MW}_m \qquad [M_p] = M_p/(\mathrm{MW}_m V_2) \tag{81}$$

Accordingly, the volume of each phase will be

$$V_1 = M_m/\rho_m \qquad V_2 = (M_p/\rho_m) + (M_0 X/\rho_p) \tag{82}$$

In stage III ($X < X_f$), the separate monomer-rich phase disappears; thus, the polymerization takes place only in the polymer-rich phase. Accordingly, the monomer distribution in the three phases will be given by the following equations

$$M_m = 0 \qquad M_p = M_0(1 - X) - M_a - M_g \tag{83}$$

$$M_g = \left(\frac{\hat{f}_m^g \mathrm{MW}_m}{RT}\right)\left[V_g(X_f) - M_0(X - X_f)\left(\frac{1}{\rho_p} - \frac{1}{\rho_m}\right)\right] \tag{84}$$

The monomer conversion, X_f, at which the monomer-rich phase disappears can be calculated from eq 71 by setting the value of M_m equal to zero. Thus, the following expression is obtained

$$X_f = \frac{X_S\left\{\dfrac{M_0 - KW_{wa} - \left[\hat{f}_m^g \mathrm{MW}_m\left(V_R - \dfrac{M_0}{\rho_m} - \dfrac{W_w}{\rho_w}\right)\right]}{RT - \left(\dfrac{\hat{f}_m^g \mathrm{MW}_m}{\rho_m} + \dfrac{\hat{f}_m^g \mathrm{MW}_m}{\rho_w}\right)}\right\}}{M_0\left[\dfrac{1 + \hat{f}_m^g \mathrm{MW}_m X_S\left(\dfrac{1}{\rho_m} - \dfrac{1}{\rho_p}\right]}{RT - \left(\dfrac{\hat{f}_m^g \mathrm{MW}_m}{\rho_m} + \dfrac{\hat{f}_m^g \mathrm{MW}_m}{\rho_w}\right)}\right]} \tag{85}$$

Diffusion-Controlled Reactions in the Polymer-Rich Phase. At high monomer conversions, almost all elementary reactions can become diffusion-controlled. Specifically, the initiation, propagation, and termination reactions have been related to the well-known phenomena of the cage, glass, and gel effects, respectively. Diffusion-controlled reactions can be described quantitatively using the generalized free-volume theory.[7]

In the present study, the simplified free-volume model of Xie et al.[7] was employed to describe diffusion-controlled reactions in the free-radical suspension polymerization of VCM. Accordingly, the diffusion-controlled termination rate constant in the polymer-rich phase, k_t^2, was expressed as follows

$$k_t^2 = k_{t0}^2 \exp\left[-A\left(\frac{1}{V_f} - \frac{1}{V_f^*}\right)\right] \tag{86}$$

where k_{t0}^2 is the termination rate constant in the polymer-rich phase for $X < X_f$. V_f is the free volume of the mixture in the polymer-rich phase, given by the equation

$$V_f = \phi_2 V_{fp} + (1 - \phi_2)V_{fm} \tag{87}$$

where V_{fp} and V_{fm} are the free volumes of the polymer and monomer, respectively. φ_2 is the volume fraction of polymer in the polymer-rich phase. V_f^* is the value of V_f at the critical monomer conversion, X_f.

Similarly, the diffusion-controlled propagation rate constant in the polymer-rich phase, k_p^2, is written as

$$k_p^2 = k_p^1 \exp\left[-B\left(\frac{1}{V_f} - \frac{1}{V_f^*}\right)\right] \tag{88}$$

where k_p^1 is the propagation rate constant in the monomer-rich phase.

Finally, the variation of the initiator efficiency with respect to the monomer conversion was calculated by the followng equation

$$(k_p^2 f^{1/2})_X = (k_p^1 f^{1/2})_{X_f} \exp\left[-B_f\left(\frac{1}{V_f} - \frac{1}{V_f^*}\right)\right] \tag{89}$$

The temperature-dependent constants A, B and B_f in eqs 86, 88, and 89 were estimated by fitting the model predictions to available experimental rate data.

Results and Discussion

The predictive capabilities of the new model were tested by a direct comparison of model predictions with a comprehensive series of experimental measurements on polymerization rate, monomer conversion, reactor pressure, etc., kindly provided by ATOFINA. The free-radical suspension polymerization of VCM was assumed to proceed under isothermal conditions in the presence of monofunctional (e.g., di(2-ethylhexyl)peroxydicarbonate (PDEH), 3-hydroxy-1,1-dimethylbutylperoxyneodecanoate (LUP610), lauroyl peroxide (LP40), etc.] and/or symmetrical bifunctional [1,3-di(2-neodecanoylperoxyisopropyl) benzene, DIPND] initiators.

In Table 2, the numerical values of the kinetic rate constants employed in the computer simulations are reported. The values of the rate constants for the chain transfer to monomer, propagation, backbiting, and termination reactions were taken from the work of

Table 2. Kinetic Rate Constants for the Free-Radical Polymerization of VCM

rate constant expression	units	ref
$k_p^1 = 3 \times 10^9 \exp(-3320/T)$	$m^3\ kmol^{-1}\ min^{-1}$	23
$k_{fm}^1 = k_{fm}^2 = 5.78 \exp(-2768/T) k_p^1$	$m^3\ kmol^{-1}\ min^{-1}$	23
$k_b^1 = k_b^2 = 0.014 k_p^1$	$m^3\ kmol^{-1}\ min^{-1}$	23
$k_t^1 = 2(k_p^1)^2/K_c$	$m^3\ kmol^{-1}\ min^{-1}$	23
$(k_t^1/k_{t0}^2)^{1/2} = 24 \exp[1007(T^{-1} - T_0^{-1})]^a$		23
$(-\Delta H_r) = 106$	kJ $kmol^{-1}$	10

[a] $T_0 = 333.15$ K.

Table 3. Physical and Thermodynamic Properties of Water, VCM, and PVC

expression	units	ref
$\rho_m = 947.1 - 1.746\theta - 3.24 \times 10^{-3}\theta^2$	kg m^{-3}	7
$\rho_w = 1011.0 - 0.4484\theta$	kg m^{-3}	7
$\rho_p = 10^3 \exp(0.4296 - 3.274 \times 10^{-4} T)$	kg m^{-3}	7
$P_w^{sat} = \exp[72.55 - 7206.7/T - 7.1386 \ln(T) + 4.046 \times 10^{-6} T^2)$	Pa	23
$P_m^{sat} = p_{cm} \exp[1/(1 - X_r)(-6.5008 X_r + 1.21422 X_r^{1.5} - 2.57867 X_r^3 - 2.00937 X_r^6)] \times 10^5$ $X_r = 1 - T/T_{cm}$	Pa	36
$T_{cm} = 425$ $T_{cw} = 647.3$	K	36
$P_{cm} = 51.5$ $P_{cw} = 221.2$	bar	36
$V_{cm} = 169$ $V_{cw} = 57.1$	$cm^3\ mol^{-1}$	36
$\omega_m = 0.122$ $\omega_w = 0.344$		36
$Z_{cm} = 0.265$ $Z_{cw} = 0.235$		36

Table 4. Parameters Used in the Diffusion Model[7]

$V_{fm} = 0.025 + a_m(T - T_{gm})$
$V_{fp} = 0.025 + a_p(T - T_{gp})$
$a_m = 9.98 \times 10^{-4}$
$a_p = 5.47 \times 10^{-4}\ K^{-1}$
$T_{gm} = 70$ K
$T_{gp} = 87.1 - 0.132(T - 273.15)$ °C

Kiparissides et al.[23] In Table 3, the physical and thermodynamic properties of the VCM/PVC/H_2O system are reported. Finally, the parameters used in the free-volume model are given in Table 4.

In Figures 4−6, experimental and model results on monomer conversion, polymerization rate, and reactor pressure, respectively, are plotted with respect to the polymerization time at three different temperatures (namely, 68.5, 58.5, and 56.5 °C). The free-radical suspension polymerization of VCM was initiated via the thermal decomposition of PDEH. In the reported runs, the initiator concentration was equal to 0.606 g/kg of VCM, and the mass ratio of water to VCM was equal to 1.55. The continuous lines represent the simulation results, and the discrete points represent the experimental measurements. It is apparent that an excellent agreement exists between the model predictions and the experimental results. The observed small discrepancies in the polymerization rate and the reactor pressure are primarily due to errors in the measurements.

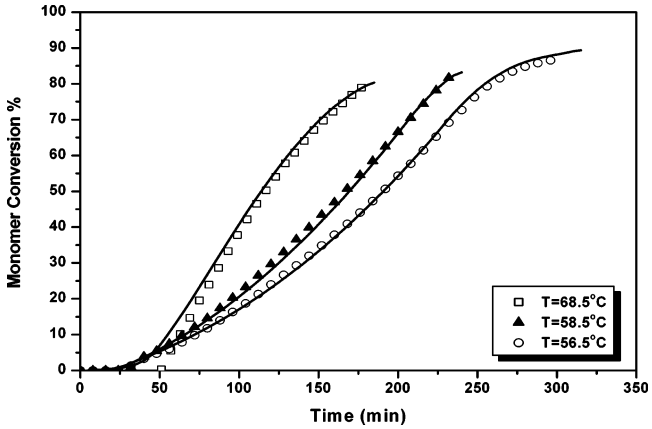

Figure 4. Predicted and experimental conversion−time histories (polymerization temperatures = 68.5, 58.5, and 56.5 °C; $M_{0,PDEH}$ = 0.606 g/kg of VCM; initial mass of water = 1.55 kg/kg of VCM).

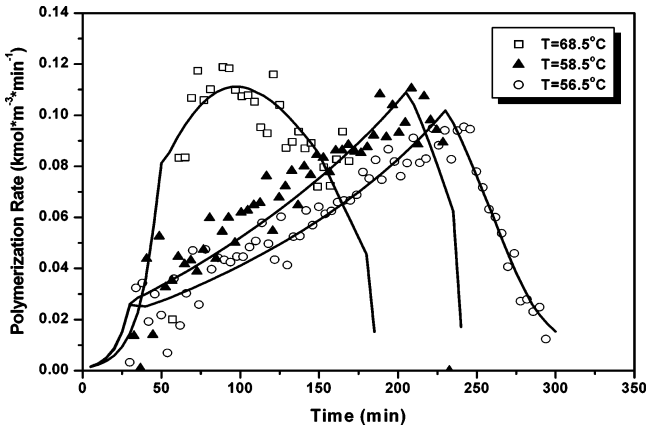

Figure 5. Predicted and experimental polymerization rate with respect to polymerization time (polymerization temperatures = 68.5, 58.5, and 56.5 °C; $M_{0,PDEH}$ = 0.606 g/kg of VCM; initial mass of water = 1.55 kg/kg of VCM).

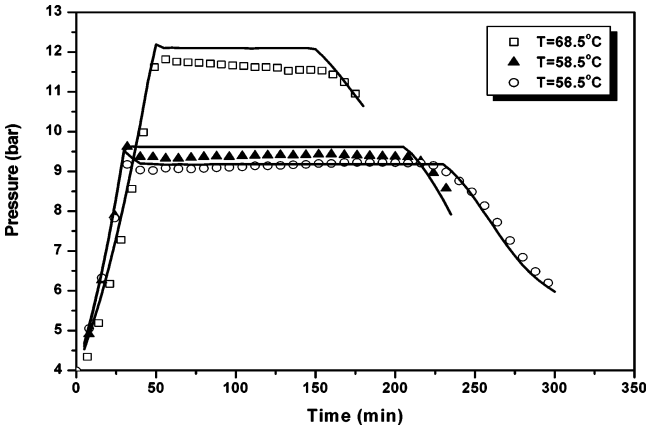

Figure 6. Predicted and experimental reactor pressures with respect to polymerization time (experimental conditions as in Figure 1).

In Figures 7 and 8, experimental and model results on monomer conversion and polymerization rate, respectively, are presented as a function of polymerization time for three different initiator loadings. In all cases, the polymerization temperature was kept constant at 56.5 °C. The polymerization was carried out in the presence of the monofunctional initiator LUP610. As can be seen, the simulation results are in good agreement with the experimental measurements.

In Figures 9 and 10, comparisons of model predictions with literature experimental data[35] on monomer conversion and number- and weight-average molecular weights, respectively, are depicted. The polymerization was carried out isothermally (T = 60 °C) in the presence of LP40 initiator. The initiator and water loadings were 2.6 g/kg of VCM and 1.7 kg/kg of VCM, respectively. As can be seen, there is an excellent agreement between model predictions and experimental data on monomer

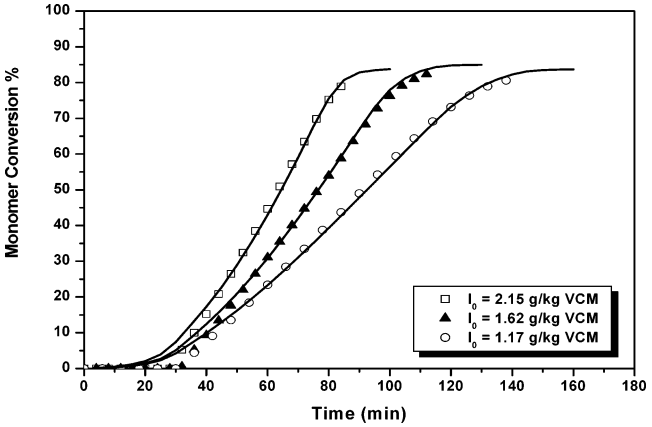

Figure 7. Predicted and experimental conversion−time histories (polymerization temperature = 56.5 °C; $M_{0,\mathrm{LUP610}}$ = 2.15, 1.62, and 1.17 g/kg of VCM; initial mass of water = 1.55 kg/kg of VCM).

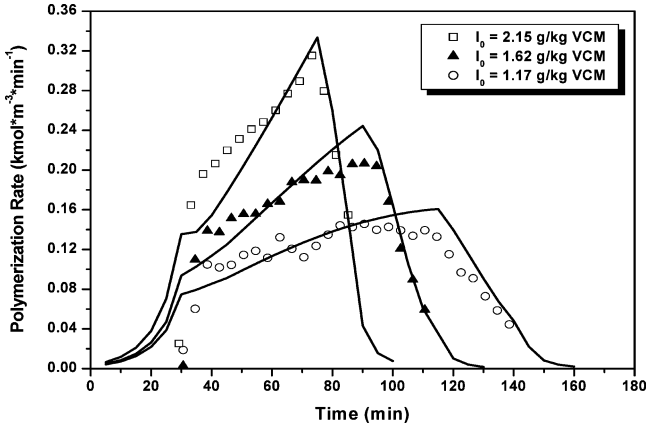

Figure 8. Predicted and experimental polymerization rates with respect to polymerization time (polymerization temperature = 56.5 °C; $M_{0,\mathrm{LUP610}}$ = 2.15, 1.62, and 1.17 g/kg of VCM; initial mass of water = 1.55 kg/kg of VCM).

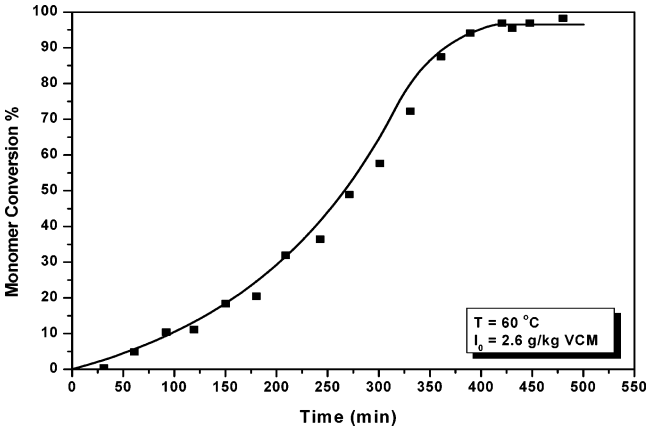

Figure 9. Predicted and experimental conversion−time histories (polymerization temperature = 60 °C, $M_{0,\mathrm{LP40}}$ = 2.6 g/kg of VCM, initial mass of water = 1.7 kg/kg of VCM).

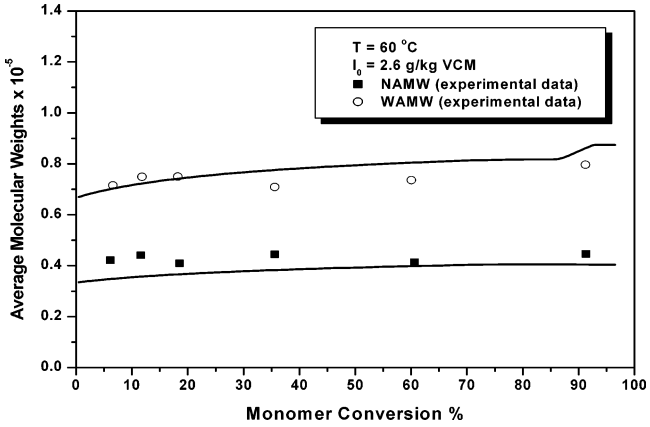

Figure 10. Predicted and experimental number- and weight-average molecular weights with respect to monomer conversion (experimental conditions as in Figure 6).

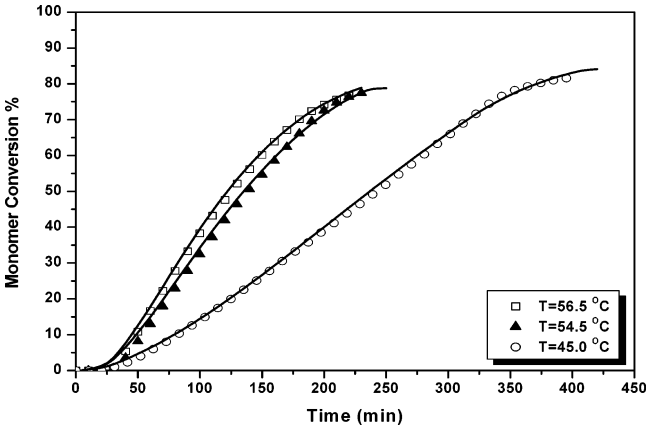

Figure 11. Predicted and experimental conversion−time histories (polymerization temperatures = 56.5, 54.5, and 45 °C; $M_{0,\mathrm{DIPND}}$ = 0.835 g/kg of VCM).

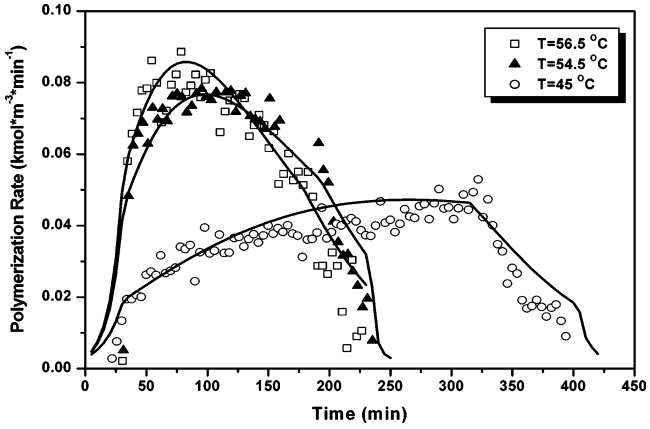

Figure 12. Predicted and experimental polymerization rates (polymerization temperatures = 56.5, 54.5, and 45 °C; $M_{0,\mathrm{DIPND}}$ = 0.835 g/kg of VCM).

conversion (Figure 9) and number- and weight-average molecular weights (Figure 10).

The proposed model was further employed to simulate the isothermal batch suspension polymerization of VCM initiated by the symmetrical bifunctional initiator DIPND. In Figures 11 and 12, comparisons of model results (continuous lines) with experimental data (discrete points) on monomer conversion and polymerization rate, respectively, are shown for three different temperatures (i.e., 45, 54.5 and 56.5 °C). In all cases, the initiator and water quantities remained the same (at 0.835 and 1.55 kg/kg of VCM, respectively). As can be seen, for all temperatures, the model predictions are in close agreement with the experimental measurements.

The present comprehensive model was also employed to simulate the free-radical polymerization of VCM initiated by a mixture of bifunctional and monofunctional initiators. In Figure 13, a comparison between model predictions and experimental measurements on monomer conversion is shown for a run carried out in the presence of a mixture of two initiators (namely,

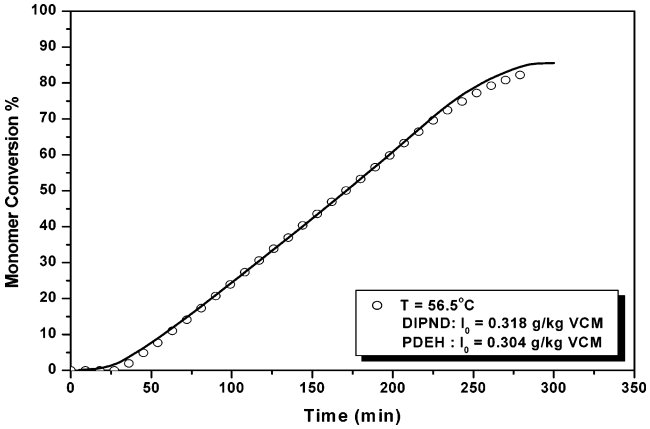

Figure 13. Predicted and experimental conversion−time histories (polymerization temperature = 56.5 °C, $M_{0,DIPND}$ = 0.318 g/kg of VCM, $M_{0,PDEH}$ = 0.304 g/kg of VCM, initial mass of water = 2.05 kg/kg of VCM).

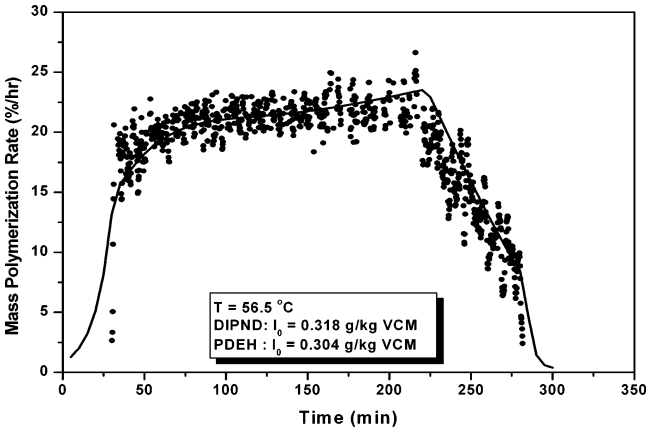

Figure 14. Predicted and experimental mass polymerization rates with respect to polymerization time (experimental conditions as in Figure 10).

0.318 g of DIPND/kg of VCM and 0.304 g of PDEH/kg of VCM) at 56.5 °C. The very good agreement between the experimental and modeling results is apparent. In Figure 14, calorimetric experimental data and model results on the polymerization rate are plotted with respect to the polymerization time. As can be seen, for the selected concentrations of DIPND and PDEH initiators, an almost-square polymerization rate profile is obtained. This means that the reactor can operate, during most of the polymerization time, at its maximum polymerization rate determined by the limited cooling capacity of the system. As a result, significant savings in the polymerization time can be achieved along with a concomitant an increase in the reactor productivity.

The effects of the initiator type (i.e., monofunctional vs bifunctional) and concentration on monomer conversion, polymerization rate, and number- and weight-average molecular weights of PVC are depicted in Figures 15−17, respectively. The simulations were carried out at 50 °C at three different concentrations of PDEH and DIPND initiators. The water loading was equal to 1.55 kg/kg of VCM. From the results of Figures 15 and 16, one can easily conclude that, for the same initiator mass loading, the VCM conversion rate for the bifunctional initiator DIPND is significantly higher than that for the monofunctional initiator PDEH. This can be explained by the higher active concentration of peroxide groups in the DIPND initiator (i.e., 3.75×10^{-3} mol of peroxide groups per gram of DIPND compared

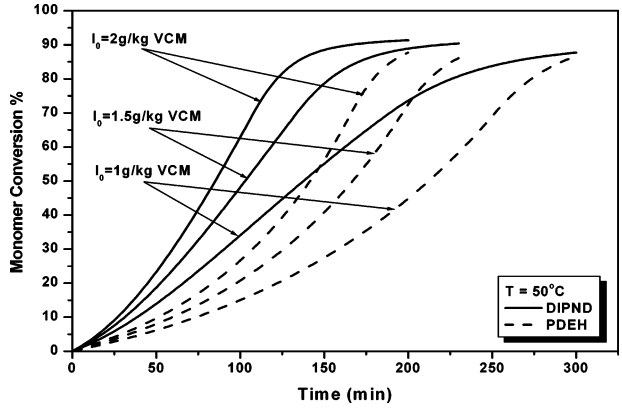

Figure 15. Predicted conversion−time histories: comparison between DIPND and PDEH initiators. (Simulation parameters: temperature = 50 °C; $M_{0,DIPND}$ = $M_{0,PDEH}$ = 1, 1.5, and 2 g/kg of VCM; initial mass of water = 1.55 kg/kg of VCM.)

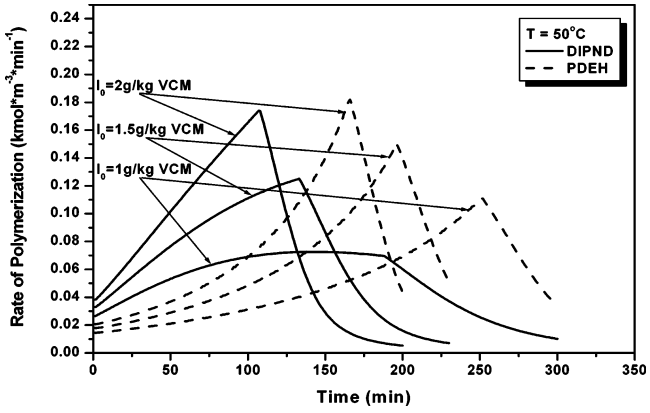

Figure 16. Predicted polymerization rates with respect to polymerization time: comparison between DIPND and PDEH initiators (operating conditions as in Figure 12).

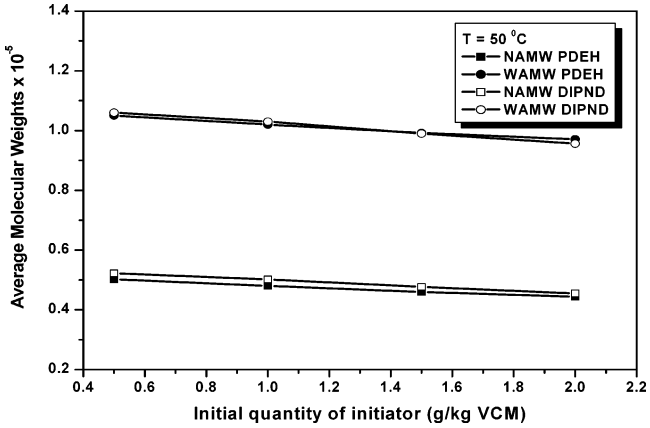

Figure 17. Predicted number- and weight-average molecular weights with respect to initiator loading: comparison between DIPND and PDEH initiators. (Simulation parameters: temperature = 50 °C, initial mass of water = 1.55 kg/kg of VCM.)

to 2.89×10^{-3} mol/g for the PDEH initiator). Notice that the initial slope of the polymerization rate for the DIPND-initiated polymerization is significantly higher than that for the PDEH initiator. As a result, a considerable reduction in the total batch polymerization time is obtained for the DIPND-initiated system. On the other hand, the number- and weight-average molecular weights do not vary significantly with respect to the initiator type (i.e, monofunctional, bifunctional) and/or concentration (Figure 17). This is due to the fact the molecular weight of PVC is mainly controlled by the

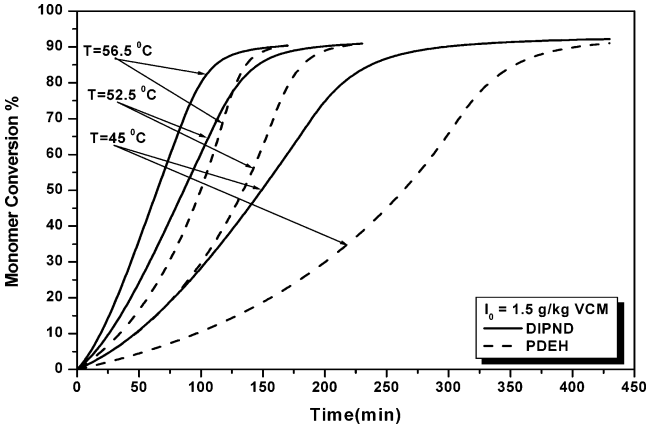

Figure 18. Predicted conversion−time histories: comparison between DIPND and PDEH initiators. (Simulation parameters: temperatures = 56.5, 52.5, and 45 °C; $M_{0,\mathrm{DIPND}} = M_{0,\mathrm{PDEH}} = 1.5$ g/kg of VCM; initial mass of water = 1.55 kg/kg of VCM.)

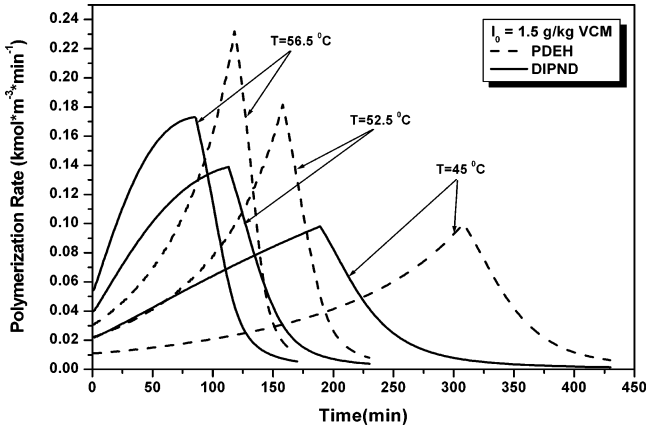

Figure 19. Predicted polymerization rates with respect to polymerization time: comparison between DIPND and PDEH initiators (operating conditions as in Figure 15).

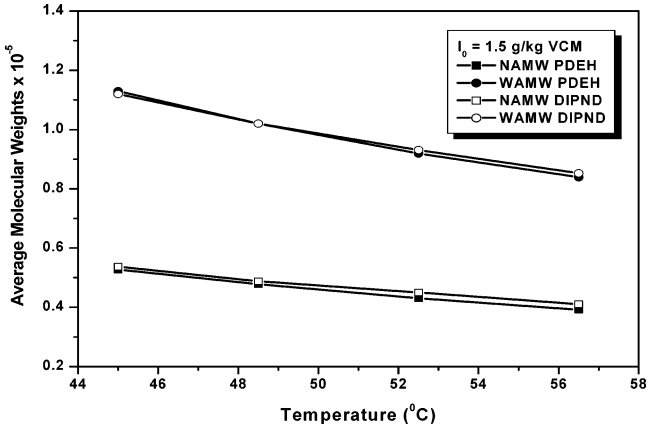

Figure 20. Predicted number- and weight-average molecular weights with respect to temperature: comparison between DIPND and PDEH initiators. (Simulation parameters: $M_{0,\mathrm{DIPND}} = M_{0,\mathrm{PDEH}} = 1.5$ g/kg, initial mass of water = 1.55 kg/kg of VCM.)

transfer to monomer reaction.[23] This means that the development of the molecular weight will primarily depend on the polymerization temperature.

Figures 18−20 show the effects of the polymerization temperature and initiator type on the monomer conversion, the polymerization rate, and the number- and weight-average molecular weights of PVC, respectively. In all simulated cases, the initiator mass loading was equal to 1.5 g/kg of VCM. It is evident that the

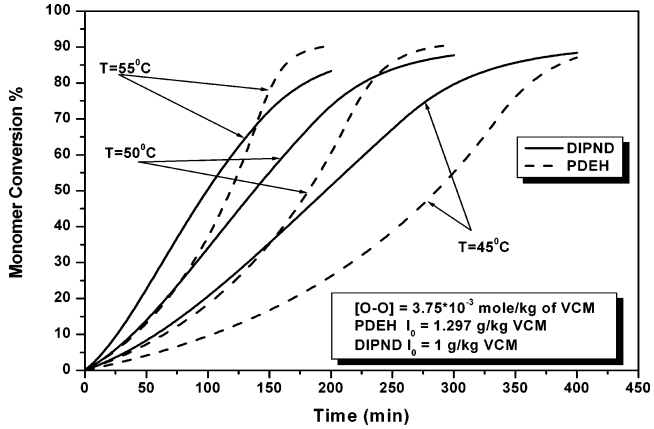

Figure 21. Predicted conversion−time histories: comparison between DIPND and PDEH initiators. (Simulation parameters: temperatures = 55, 50, and 45 °C; $M_{0,\mathrm{DIPND}} = 1$ g/kg of VCM, $M_{0,\mathrm{PDEH}} = 1.297$ g/kg of VCM; initial mass of water = 1.55 kg/kg of VCM.)

polymerization rate increases with temperature, leading to a corresponding decrease of the batch polymerization time (i.e., increase of the reactor productivity). Notice that, for the same initiator mass loading, the polymerization rate profile with respect to time for the DIPND-initiated polymerization is smoother than that for the PDEH-initiated system. It is important to point out that, because of the more favorable formation of radicals obtained in the presence of DIPND, the maximum value of the polymerization rate is considerable lower than that for the PDEH-initiated system. As a result, the maximum heat-transfer requirements for the DIPND-initiated polymerization system will be lower than those required for the PDEH-initiated system. In fact, in the presence of the PDEH initiator, the polymerization of VCM might not be possible to carry out in a batch reactor at 56.5 °C because of heat-transfer limitations [i.e., the reactor cooling capacity rate might be lower than the heat generated at the peak value of the polymerization rate, $UA\Delta T_{\mathrm{mean}} < (-\Delta H_{\mathrm{r,T}})V_{\mathrm{r}}r_{\mathrm{p,max}}$]. On the other hand, the polymerization can easily be carried out in the presence of the DIPND initiator because the corresponding polymerization rate is lower than that of the PDEH-initiated system (Figure 19). Finally, in Figure 20, the effect of the polymerization temperature on the number- and weight-average molecular weights of PVC is shown for the two initiators. It is apparent that the number- and weight-average molecular weights decrease as the polymerization temperature increases. On the other hand, at the same polymerization temperature, the initiator type does not significantly affect the values of M_{n} and M_{w} because their values depend mainly on the transfer to monomer rate constant.

Figures 21−23 show the effects of the initiator type (i.e., DIPND, PDEH) and polymerization temperature on monomer conversion, polymerization rate, and number- and weight-average molecular weights, respectively. In all simulated runs, the molar concentration of peroxide groups [−O−O−] was equal to 3.75×10^{-3} mol/kg of VCM. This means that the mass loading was larger for PDEH than for the DIPND initiator (i.e., 1.297 g of PDEH/kg of VCM versus 1 g of DIPND/kg of VCM). From the results of Figures 21 and 22, one can easily observe that, at lower polymerization temperatures (i.e., 45 °C), the rate of monomer conversion for the DIPND-initiated system is significantly higher than that for the PDEH-initiated system despite the fact that the initial

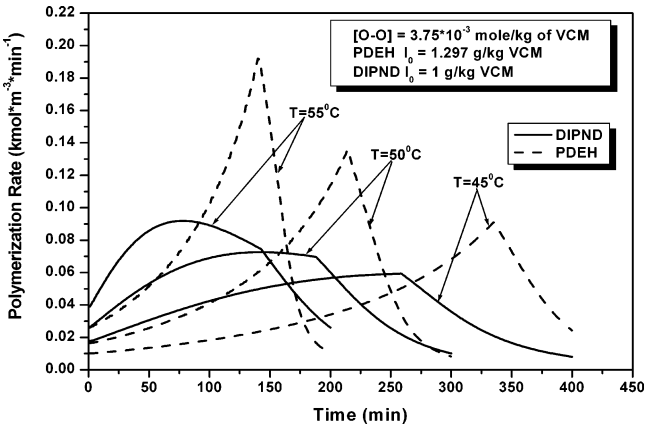

Figure 22. Predicted polymerization rates with respect to polymerization time: comparison between DIPND and PDEH initiators (operating conditions as in Figure 18).

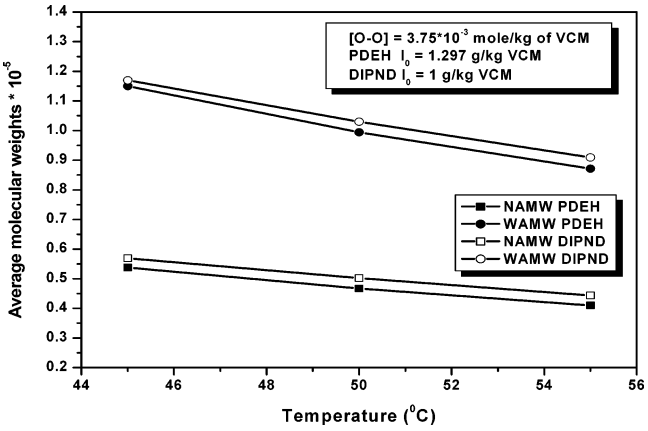

Figure 23. Predicted number- and weight-average molecular weights with respect to temperature: comparison between DIPND and PDEH initiators (operating conditions as in Figure 18).

mass loading of DIPND is smaller than that of PDEH. This behavior is due to the lower activation energy of the bifunctional initiator (i.e., $E/R = 10830$ K for DIPND versus $E/R = 14407$ K for PDEH). On the other hand, at higher polymerization temperatures, the batch polymerization time required to reach the final monomer conversion for the PDEH-initiated system is lower than that for the DIPND-initiated system, which is largely because of the lower overall initiator efficiency of DIPND. However, it should be emphasized that the use of the DIPND bifunctional initiator results in a more rounded polymerization profile that significantly lowers the heat-removal requirements of the batch reactor. Moreover, in the presence of the DIPND initiator, the number- and weight-average molecular weights of PVC increase by 5−8% over the corresponding values for the PDEH system.

Conclusions

A comprehensive mathematical model has been developed to describe the free-radical polymerization of vinyl chloride in the presence of monofunctional and bifunctional initiators. The predictive capabilities of the proposed model were demonstrated by the successful simulation of experimental measurements on VCM conversion, polymerization rate, pressure, and number- and weight-average molecular weights over a wide range of temperatures and initiator concentrations.

On the basis of the above simulation results, one can conclude that the use of bifunctional initiators can result in a considerable decrease of the batch polymerization time while keeping the maximum value of the polymerization rate below the cooling capacity limit of the reactor. Moreover, the smoother polymerization rate profile obtained with the DIPND initiator significantly improves the control of the polymerization temperature, which, in turn, enhances the safety of the VCM suspension polymerization process.

Notation

General

A = constant used in the free-volume theory for the calculation of the diffusion-controlled termination reaction
a_m = monomer activity
B_m = virial coefficient of monomer
B_{mw} = virial coefficient of a mixture of VCM and water
B_w = virial coefficient of water
D_n = dead polymer chain of length n
DIPND = 1,3-di(2-neodecanoylperoxyisopropyl) benzene
f_b = Initiator efficiency for bifunctional initiator
f_{bA} = initiator efficiency associated with the initiation of active polymer chains R_A, R_B, and R
f_{bB} = initiator efficiency associated with the initiation of inactive polymer chains U_n, V_n, W_n, U'_n, and V'_n
f_i = initiator efficiency for a monofunctional initiator of type i
f_{ir} = fraction of new macroradicals formed via the decomposition of the molecular species Q_n, S_n, U_n, U'_n, V_n, V'_n, and W_n
$\hat{f}$ = fugacity, Pa
I_b = bifunctional initiator
$I_{m,i}$ = monofunctional initiator of type i
k_{dA}^j = decomposition rate constant associated with peroxide group A in phase j, min^{-1}
k_{dB}^j = decomposition rate constant associated with peroxide group B in phase j, min^{-1}
k_I^j = initiation rate constant in phase j, m^3/(kmol min)
k_p^j = propagation rate constant in phase j, m^3/(kmol min)
k_{fm}^j = chain transfer to monomer rate constant in phase j, m^3/(kmol min)
k_b^j = intramolecular transfer rate constant in phase j, min^{-1}
k_{tc}^j = termination by combination rate constant in phase j, m^3/(kmol min)
k_{td}^j = termination by disproportionation rate constant in phase j, m^3/(kmol min)
k_z^j = inhibition rate constant in phase j, m^3/(kmol min)
K = Solubility constant of VCM in the water phase
k_t^1 = termination rate constant in the monomer-rich phase, m^3/(kmol min)
k_t^2 = termination rate constant in the polymer-rich phase, taking into account the effect of
the diffusion of polymer chains, m^3/(kmol min)
k_{t0}^2 = termination rate constant in the polymer-rich phase, m^3/(kmol min)
LUP610 = 3-hydroxy-1,1-dimethylbutylperoxyneodecanoate
LP40 = layroyl peroxide
M = mass of VCM, kg
M_0 = initial mass of VCM, kg
M_n = number-average molecular weight, kg/kmol
M_w = weight-average molecular weight, kg/kmol
MW_m = molecular weight of VCM, kg/kmol
MW_w = molecular weight of water, kg/kmol
N_m = number of monofunctional initiators
P = total reactor pressure, Pa

PD = polydispersity index
P_m = VCM partial pressure, Pa
P_n = live polymer chain of length n
P_w^{sat} = water saturation pressure, Pa
PDEH = di(2-ethylhexyl)peroxydicarbonate
Q_n = live polymer chain of length n with one terminal peroxide group of type A
R = primary radical not containing a peroxide group
R = ideal gas constant, kJ/(kmol min)
R_A = primary radical with one terminal peroxide group of type A
R_B = primary radical with one terminal peroxide group of type B
R′ = primary diradical species
$r_{\lambda,x}$ = moment function of polymer species x
S_n = live polymer chain of length n with one terminal peroxide group of type B
SCB = concentration of short chain branches per molecule, kmol/m^3
T = reactor temperature, K
T_n = diradical-line polymer chain of length n
TDB = concentration of terminal double bonds per molecule, kmol/m^3
U_n = inactive polymer chain of length n with one terminal peroxide group of type A
U'_n = inactive polymer chain of length n with two terminal peroxide groups (A and A)
V = volume of the dispersed phase, m^3
V_n = inactive polymer chain of length n with one terminal peroxide group of type A
V'_n = inactive polymer chain of length n with two terminal peroxide groups (B and B)
V_j = volume of phase j, m^3
V_g = volume of the gas phase, m^3
V_R = total reactor volume, m^3
V_f = free volume of the mixture
V_f^* = free volume of the mixture at the critical conversion
V_{fp} = free volume of polymer
V_{fm} = free volume of monomer
VCM = vinyl chloride monomer
W_n = inactive polymer chain of length n with two terminal peroxide groups (A and B)
W_w = total mass of water, kg
W_{wa} = mass of water in the aqueous phase, kg
X = monomer conversion
X_f = critical conversion
y_m = mole fraction of monomer in the gas phase
y_w = mole fraction of water in the gas phase
Z = inhibitor

Greek Letters

δ_{mw} = monomer solubility in the aqueous phase
$\lambda_{\xi,k}$ = moment function of order k associated with live polymer chains
$\lambda_{\theta,k}$ = moment function of order k associated with inactive polymer chains
μ_k = moment function of order k associated with dead polymer chains
ρ_m = VCM density, kg/m^3
ρ_p = polymer density, kg/m^3
ϕ_m = fugacity coefficient of monomer
φ_i = volume fraction of substance i in the dispersed phase
$\varphi_{2,c}$ = volume fraction of polymer in the dispersed phase at the critical conversion
χ = Flory−Huggins interaction parameter

Subscripts

a = aqueous phase
f = critical
g = gas phase
i = initiator
m = monomer phase
p = polymer phase

Superscripts

j = phase j
m = monomer phase
p = polymer phase
g = gas phase
w = aqueous phase

Literature Cited

(1) Smallwood, P. V. Vinyl Chloride Polymers, Polymerization. In *Encyclopedia of Polymer Science and Technology*; Mark, H., Ed.; Wiley: New York, 1990; Vol. 17, p 295.

(2) Saeki, Y.; Emura, T. Technical progresses for PVC production. *Prog. Polym. Sci.* **2002**, *27*, 2055.

(3) Burgess, R. H. *Manufacturing and Processing of PVC*; Applied Science Publishers: London, 1982.

(4) Langsam, M. In *Encyclopedia of PVC*, 2nd ed.; Nass, L. I., Heiberger, C. A., Eds.; Marcel Dekker Inc.: New York, 1986; Vol. 1, p 48.

(5) Tornell, B. E. Recent Developments in PVC Polymerization. *Polym. Plast. Technol. Eng.* **1988**, *27*, 1.

(6) Xie, T. Y.; Hamielec, A. E.; Wood, P. E.; Woods, D. R. Suspension, Bulk and Emulsion Polymerization of Vinyl Chloride—Mechanism, Kinetics and Modelling. *J. Vinyl Technol.* **1991**, *13* (1), 2.

(7) Xie, T. Y.; Hamielec, A. E.; Wood, P. E.; Woods, D. R. Experimental Investigation of Vinyl Chloride Polymerization at High Conversion: Mechanism, Kinetics and Modelling. *Polymer* **1991**, *32* (3), 537.

(8) Yuan, H. G.; Kalfas, G.; Ray, W. H. Suspension Polymerization. *J. Macrom. Sci., Rev. Macromol. Chem. Phys.* **1991**, *C31* (2&3), 215.

(9) Mejdell, T.; Pettersen, T.; Naustdal, C.; Svendsen, H. F. Modelling of Industrial S−PVC Reactor. *Chem. Eng. Sci.* **1999**, *54*, 2459.

(10) Sidiropoulou, E.; Kiparissides, C. Mathematical Modelling of PVC Suspension Polymerization. *J. Makromol. Sci., Chem.* **1990**, *A27* (3), 257.

(11) Abdel-Alim, A. H.; Hamielec, A. E. Bulk Polymerization of Vinyl Chloride. *J. Appl. Polym. Sci.* **1972**, *16*, 783.

(12) Kuchanov, S. I.; Bort, G. C. Kinetics and Mechanism of Polymerization of Vinyl Chloride. *Polym. Sci.* **1973**, *A15*, 2712.

(13) Ray, W. H.; Jain, S. K.; Salovey, R. On the Modelling of Bulk PVC Reactors. *J. Appl. Polym. Sci.* **1975**, *19*, 1297.

(14) Ugelstad, J.; Moerk, P. C.; Hansen, F. K.; Kaggerund, K. H.; Ellingsen, T. Kinetics and Mechanism of Vinyl Chloride Polymerization. *Pure Appl. Chem.* **1981**, *53*, 323.

(15) Chan, R. K. S.; Langsam, M.; Hamielec, A. E. Calculation and Applycations of VCM Distribution in Vapor/Water/Solid Phase during VCM Polymerization. *J. Macromol. Sci. Chem.* **1982**, *A17* (6), 969.

(16) Hamielec, A. E.; Gomez-Vaillard, R.; Marten, F. L. Diffusion Controlled Free Radical Polymerization. Effect on Polymerization Rate and Molecular Properties of PVC. *J. Macromol. Sci. Chem.* **1982**, *A17* (6), 1005.

(17) Kelsall, D. C.; Maitland, G. C. The interaction of process conditions and product properties for PVC. In *Polymer Reaction Engineering*; Reichert, K. H., Geiseler, W., Eds.; VCH Publishers: Berlin, 1983; p 133.

(18) Weickert, G.; Henschel, G.; Weissenborn, K. D. Kinetik der VC Polymerisation Ein modellvergleich—I. Modellselektion. *Angew. Makromol. Chem.* **1987**, *147*, 1.

(19) Weickert, G.; Henschel, G.; Weissenborn, K. D. Kinetik der VC Polymerisation Ein modellvergleich—II. Anwendongsbeispiele. *Angew. Makromol. Chem.* **1987**, *147*, 19.

(20) Xie, T. Y.; Hamielec, A. E.; Wood, P. E.; Woods, D. R. Experimental Investigation of Vinyl Chloride Polymerization at High Conversion: Reactor Dynamics. *J. Appl. Polym. Sci.* **1991**, *43*, 1259.

(21) Dimian, A.; Van Diepen, D.; Van der Wal, G. A. Dynamic Simulation of a PVC Suspension Reactor. *Comput. Chem. Eng.* **1995**, *19S*, S427.

(22) Lewin, D. R. Modelling and Control of an Industrial PVC Suspension Polymerization Reactor. *Comput. Chem. Eng.* **1996**, *20*, S865.

(23) Kiparissides, C.; Daskalakis, G.; Achilias, D. S.; Sidiropoulou, E. Dynamic Simulation of Industrial Poly(vinyl chloride) Batch Suspension Polymerization Reactors. *Ind. Eng. Chem. Res.* **1997**, *36*, 1253.

(24) Kim, K. J.; Choi, K. Y. Modeling of Free Radical Polymerization of Styrene Catalyzed by Unsymmetrical Bifunctional Initiators. *Chem. Eng. Sci.* **1989**, *44*, 297.

(25) Villalobos, M. A.; Hamielec, A. E.; Wood, P. E. Kinetic Model for Short-Cycle Bulk Styrene Polymerization through Bifunctional Initiators. *J. Appl. Polym. Sci.* **1991**, *42*, 629.

(26) Villalobos, M. A.; Hamielec, A. E.; Wood, P. E. Bulk and Suspension Polymerization of Styrene in the Presence of *n*-Pentane. An Evaluation of Monofunctional and Bifunctional Initiation. *J. Appl. Polym. Sci.* **1993**, *50*, 327.

(27) Estenoz, D. A.; Leal, G. P.; Lopez, Y. R.; Oliva, H. M.; Meira, G. R. Bulk Polymerization of Styrene in the Presence of Polybutadiene. The Use of Bifunctional Initiators. *J. Appl. Polym. Sci.* **1996**, *62*, 917.

(28) Gonzalez, I. M.; Meira, G. R.; Oliva, H. M. Synthesis of Polystyrene with Mixtures of Mono- and Bifunctional Initiators. *J. Appl. Polym. Sci.* **1996**, *59*, 1015.

(29) Dhib, R.; Al-Nidawy, N. Modelling of Free Radical Polymerization of Ethylene Using Difunctional Initiators. *Chem. Eng. Sci.* **2002**, *57*, 2735.

(30) Starnes, W. H., Jr.; Zaikov, V. C.; Chung, H. T.; Wojciechowski, B. J.; Tran, H. V.; Saylor, K. Intramolecular Hydrogen Transfers in Vinyl Chloride Polymerization: Routes to Doubly Branched Structures and Internal Double Bonds. *Macromolecules* **1998**, *31*, 1508.

(31) Starnes, W. H., Jr. Structural and Mechanistic Aspects of the Thermal Degradation of Poly(vinyl chloride). *Prog. Polym. Sci.* **2002**, *27*, 2133.

(32) Achilias, D. S.; Kiparissides C. Development of a General Mathematical Framework for Modelling of Diffusion-Controlled Free-Radical Polymerization Reactions. *Macromolecules* **1992**, *25*, 3739.

(33) Xie, T. Y.; Hamielec, A. E.; Wood, P. E.; Woods, D. R. Experimental investigation of vinyl chloride polymerization at high conversion—Temperature/pressure/conversion and monomer phase distribution relationships. *J. Appl. Polym. Sci.* **1987**, *34*, 1749.

(34) Nilsson, H.; Silvegren, C.; Tornell, B. Swelling of PVC Latex Particles by VCM. *Eur. Polym. J.* **1978**, *14*, 737.

(35) Cebollada, A. F.; Schmidt, M. J.; Farber, J. N.; Capiati, N. J.; Valles, E. M. Suspension Polymerization of Vinyl Chloride. I. Influence of Viscosity of Suspension Medium on Resin Properties. *J. Appl. Polym. Sci.* **1989**, *37*, 145.

(36) Reid, R. C.; Prausnitz, B. E.; Poling, B. E. *The Properties of Gases and Liquids*, 4th ed.; McGraw-Hill International Editions, Singapore, 1988; p 212.

Received for review February 10, 2004
Revised manuscript received June 22, 2004
Accepted June 28, 2004

IE0498908